Prediction of Velocity Distribution from the Statistics of Pore Structure in 3D Porous Media via High-Fidelity Pore-Scale Simulation

by

Mohammad S Kh F Sh AlAdwani

Submitted to the Center for Computational Engineering (CCE) and the Department of Electrical Engineering and Computer Science (EECS) in partial fulfillment of the requirements for the degrees of

Master of Science in Computation for Design and Optimization and Master of Science in Electrical Engineering and Computer Science

at the

MASSACHUSETTS INSTITUTE OF TECHNOLOGY

September 2017

Author ..... Signature redacted
Center for Computational Engineering (CCE) and the
Department of Electrical Engineering and Computer Science (EECS)
August 31, 2017

Certified by ..... Signature redacted .....
Ruben Juanes
Associate Professor, Department of Civil an Environmental Engineering
Thesis Supervisor

Certified by ..... Signature redacted
Jongyoon Han
Professor, Department of Electrical Engineering and Computer Science
Thesis Reader

Accepted by ..... Signature redacted .....
Nicolas Hadjiconstantinou
Professor, Department of Mechanical Engineering
Co-Director, Computation for Design and Optimization

Accepted by ..... Signature redacted .....
Leslie A Kolodziejski
Professor, Department of Electrical Engineering and Computer Science
Chair, Department Committee on Graduate Students

Prediction of Velocity Distribution from the Statistics of Pore Structure in 3D Porous Media via High-Fidelity Pore-Scale Simulation

by

Mohammad S Kh F Sh AlAdwani

Submitted to the Center for Computational Engineering (CCE) and the
Department of Electrical Engineering and Computer Science (EECS)
on August 31, 2017, in partial fulfillment of the
requirements for the degrees of
Master of Science in Computation for Design and Optimization and
Master of Science in Electrical Engineering and Computer Science

Abstract

Fluid flow and particle transport through porous media are determined by the geometry of the host medium itself. Despite the fundamental importance of the velocity distribution in controlling early-time and late-time transport properties (e.g., early breakthrough and superdiffusive spreading), direct relations linking velocity distribution with the statistics of pore structure in 3D porous media have not been established yet. High velocities are controlled by the formation of channels, while low velocities are dominated by stagnation zones. Recent studies have proposed phenomenological models for the distribution of high velocities including stretched exponential and power-exponential distributions but without an underlying mechanistic or statistical physics theory.

Here, we investigate the relationship between the structure of the host medium and the resulting fluid flow in random dense spherical packs. We simulate flow at low Reynolds numbers by solving the Stokes equations with the finite volume method and imposing a no-slip boundary condition at the boundary of each sphere. High fidelity numerical simulations of Stokes flow are facilitated with the assist of open source Computational Fluid Dynamics (CFD) tools such as OpenFOAM. We show that the distribution of low velocities in 3D porous media is described by a Gamma distribution, which is robust to variations in the geometry of the porous media. We develop a simple model that predicts the parameters of the gamma distribution in terms of the porosity of the host medium. Despite its simplicity, the analytical predictions from the model agree well with high-resolution simulations in terms of velocity distribution.

Thesis Supervisor: Ruben Juanes
Title: Associate Professor of Civil and Environmental Engineering

Acknowledgments

First and foremost, I would like to thank God for all the blessings bestowed on me. Without the support and continued guidance from a higher power, I would not be in the privileged position that I find myself in today. I would also like to thank my mother, thank you very much for your support and bringing out the best in me. Words fail to express my deep gratitude and love to you. Your wisdom, encouragement, and love have kept me going and has made me a stronger and wiser person. I wish to present my special thanks to my research advisor, Ruben Juanes. Thank you for introducing me to a wonderful research area and giving me the opportunity to shine. Working and learning from you will always be one of the most memorable aspects of this program. You have made my journey in this program a fruitful one.

I would also like to extend my appreciation to the Prime Minister of Kuwait, Sheikh Jaber Al-Mubarak Al-Hamad Al-Sabah, for his financial support towards my education. Special thanks go to Abdulaziz Al-Baiz for the efforts and guidance throughout the years. To the former administrator staff at the CDO program, Sydney Miller, thank you very much for your kindness, encouragement and help when I needed it. To the members of the Juanes Group, especially, Zhibing Yang for all the help with the generation of synthetic porous media in PFC. To my friend and my colleague, Abdelaziz Beljadid, thank you for your warm hospitality and providing me with a great working environment. Moreover, I would like to thank Leslie Kolodziejski and my thesis reader, Jongyoon Han, for supporting me in the EECS department. Many thanks go to the Center for Computational Engineering (CCE) and the department of Electrical Engineering and Computer Science (EECS); I had a productive time being a student in both departments for the past few years.

Contents

List of Figures

List of Tables

Chapter 1

Introduction

1.1 Motivation and Overview

A porous medium is a material that consists of a solid portion with void spaces or holes within it. The solid matrix (mineral grains in soils and rocks) can either be rigid, which is the usual situation, or can undergo small deformations. The void spaces or pores in the porous medium allow the flow of fluids through them. The macroscopic behavior of flow systems is ultimately determined by flow and transport at the pore scale within the void space left by the solid fraction. The pores are assumed to be interconnected, meaning that there exist many continuous paths from one side of the medium to the other [2]. In a typical porous medium, the pores are relatively narrow and their distribution with respect to size and shape is irregular; hence, flow quantities, such as velocities and pressures at the pore-scale (the microscopic scale) are not easily predicted from the statistics of the pore structures directly. Such irregularities within complex pore networks that have many cavities rule out conventional approaches to quantify velocities of fluids in a porous medium. Measurements of global quantities (e.g., porosity, permeability, conductivity) along with computational tools are useful in describing fluid velocities in a more simplistic manner, thus working around limitations. Connecting such quantities with fluid velocities, which are obtained from simulation results are not fully developed in single phase flow, where the pores are filled with a single fluid. In multiphase flow, the pores are shared by liquids and/or gases and the difficulty of predicting flow quantities from the statistics of pore structures escalates drastically.

Detailed knowledge of flow in complex porous systems is important, as it is relevant in several natural and industrial engineered processes. Examples include containing and/or remediating soil and groundwater contamination [1,2], fluid infiltration in porous systems [6], geologic carbon sequestration [4], enhanced hydrocarbon recovery [5], water filtration in heterogeneous soil [3] and fuel cells [7]. Semi-empirical relations between permeability and porosity have been developed and validated for certain media [8-11]. However, many open theoretical challenges exist to determine the fluid velocity distributions from statistical descriptions of pore-scale geometry. The quantification of the velocity field in heterogeneous porous media is a challenging problem and has many applications, since it affects particle distribution [12–18] and controls mixing of fluids [19–22], which can further promote both chemical reactions [23–27] and biological activity [28, 29]. Numerical modelling at the pore scale has shown the appearance of highly heterogeneous velocity distributions, even in simple homogeneous porous media [17, 31, 32, 39–41]. These velocity distributions have also been observed in laboratory and field experiments such as on bead packs [30–35], sand columns [36] and real rock samples [37, 38].

It is well known that particle-transport through porous media is often anomalous, meaning that it is dominated by highly heterogeneous velocity distributions and is characterized by heavy-tailed solute breakthrough curves, and nonlinear temporal evolution of particle mean square displacement (MSD). These behaviors can be captured via high resolution pore-scale simulations or direct experimental observations. Distinct behaviors for different velocity scales have been identified via computational modelling [17, 39, 40, 42, 43] and experimental tests [34, 35, 38]. These studies have shown that low velocities are dominated by stagnation zones, while high velocities are controlled by the formation of channels in the medium. Several studies have shown

that high velocities are explained by exponential [44] and power-exponential [43] distributions, but without a clear physical justification. Asymptotic transport properties [12, 42] are known to be influenced by the distribution of low velocities. The ability to quantify flow heterogeneity, with an emphasis on low velocities, from the statistics of the porous medium alone would be an important element towards better predictions of flow and transport processes in subsurface environments.

1.2 Thesis Outline

In this thesis, Chapter 2 describes the software architecture for performing high-resolution simulations of Stokes equations; from generating 3D porous media that are composed of random dense sphere packs all the way to the process of how to handle geometry data and put in a suitable format that is compatible with OpenFOAM, which is an open source Computational Fluid Dynamics tool that is capable of solving for velocity fields and pressure everywhere in the porous media's void spaces. The chapter also gives a brief overview of the meshing process of the spaces and how the flow quantities that are produced by OpenFOAM are post-processed for analysis. Chapter 3 presents the results obtained by following the procedures in the preceding chapter. Visualization of both the velocity fields and the pressure everywhere in the generated porous media will be included along with the probability density function (PDF) of the rescaled velocity magnitudes everywhere in the host media. We show that this PDF is described by a Gamma distribution, which is robust to variations in the geometry of the porous media. In the same chapter, we develop a simple model that predicts the parameters of the gamma distribution in terms of the porosity of the host medium and show that the analytical predictions from the model agree well with high-resolution simulations in terms of the velocity distribution. The same chapter provides

a discussion as well as a theoretical justification of some of the obtained results. A summary of this thesis and a conclusion of its findings are presented in Chapter 4.

Chapter 2

Methodology: Software Architecture of 3D High-Fidelity Simulations of Stokes Equations

2.1 Stokes Flow

In a 3D porous medium, assume that the flow is incompressible and steady within the pore geometry. The flow is assumed to be horizontal; therefore, the gravitational term is neglected. When the flow is simulated at low Reynolds numbers (ratio of inertial to viscous forces) $Re \ll 1$, the flow is Stokesian and is described by the following equations

$$\nabla \cdot \boldsymbol{u} = 0 \tag{2.1}$$

$$\mu \nabla^2 \boldsymbol{u} = \nabla p \tag{2.2}$$

Here, p is the fluid pressure, $\boldsymbol{u}$ is the fluid velocity and μ is the dynamic viscosity of the fluid. Eq. (2.1) is the incompressibility condition of the fluid, which states that the velocity field is divergence-free while Eq. (2.2) is the conservation of momentum equation for fluids simplified by the assumptions mentioned earlier. Assume that the 3D porous medium of interest is bounded by a cubic container and assume that the flow is driven by a single pressure gradient from one side of the bounding box ($\partial\Omega_{inlet}$) to the opposite side ($\partial\Omega_{outlet}$). No-slip boundary conditions are imposed at the remaining four surfaces of the bounding box ($\partial\Omega_{rest}$) as well as at the surface of the porous medium's solid matrix, which will be assumed to be spherical in shape ($\partial\Omega_{spheres}$). These boundary conditions translate into the following relations.

$$p = 1, \qquad \boldsymbol{u} \cdot \boldsymbol{t} = 0 \qquad \text{in } \partial\Omega_{inlet} \tag{2.3}$$

$$p = 0, \qquad \boldsymbol{u} \cdot \boldsymbol{t} = 0 \qquad \text{in } \partial\Omega_{outlet} \tag{2.4}$$

$$\nabla p \cdot \boldsymbol{n} = 0, \qquad \boldsymbol{u} = \boldsymbol{0} \qquad \text{in } \partial\Omega_{rest} \cup \partial\Omega_{spheres} \tag{2.5}$$

Here, $\boldsymbol{n}$ and $\boldsymbol{t}$ are unit vectors normal and tangent to the surface of interest respectively. Due to the linearity of Stokes equations, the choices for the fixed pressures in Eq. (2.3) and Eq. (2.4) can be arbitrary. In both equation, the tangential velocities at the inlet and outlet are set to be zero as the flow is horizontal on both surfaces. Eq. (2.5) is the no-slip boundary condition described mathematically.

2.2 Software Architecture

In this section, the methodology of performing high-fidelity simulations of Stokes equations is described. The procedure can be summarized into five steps and the software tools used at each step along with the associated functions are included as follows.

- **Particle Flow Code or PFC:** The software generates random dense sphere packs. The coordinates of each sphere along with the corresponding radius are outputted from PFC.
- **Gmsh**: This mesh generator takes the output of PFC, triangulates the spherical surfaces of the dense sphere pack and outputs it in a Stereolithography (STL) format.
- **BlockMesh and SnappyHexMesh**: The STL file of the triangulated surface geometries from Gmsh is used to create high-quality meshes of the void spaces in the porous medium.
- **OpenFOAM**: From the 3D mesh created by snappyHexMesh, the software solves Stokes equations (2.1) and (2.2) with the specified boundary conditions (2.3), (2.4) and (2.5).
- **ParaView**: It is a visualization tool that displays the pressure and velocity fields outputted from OpenFOAM everywhere at the pores of the 3D host medium.

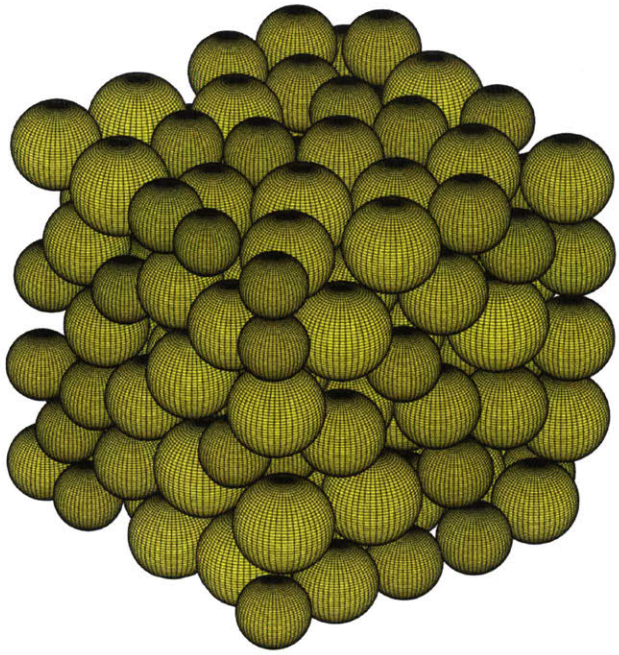

Figure 2-1: An example of a 3D porous medium composed of random sphere packs that is generated by PFC inside a cubic container of volume $125mm^3$.

2.2.1 Generation of the Sphere Packs

The first step in simulating Stokes equations is generating an appropriate 3D porous medium. Several porous media have been generated in this study via the numerical "Particle Flow Code" or PFC [45]. PFC is a software that models the movement and interaction of spherical particles using the discrete element method. Via highly efficient algorithms incorporated in the software, the tool has been used to generate random sphere packs inside a cubic box of volume $125mm^3$. Several algorithms [46-48] exist that generate spherical particles and pack them in a container; however, PFC generates the spherical packs via the algorithm [49] which generates small balls that are enlarged until they fully fill the domain. The balls are then subjected to the action of gravity, where they can fall and roll until reaching a stable state. The spheres are also generated so that the appearance of obtuse angles in the Delaunay triangulation of the spheres' centers is minimized.

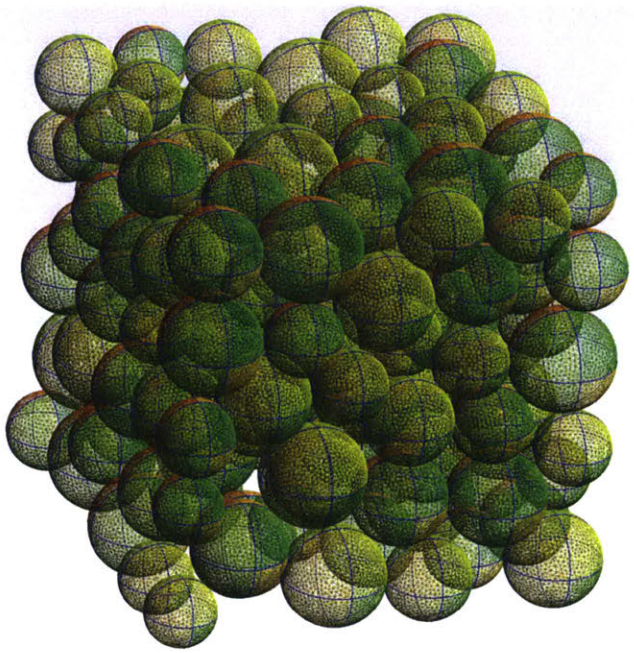

Figure 2-2: An example of a dense sphere pack bounded by a cubic box of volume $125mm^3$ with its surface being meshed and triangulated by the software Gmsh.

2.2.2 Meshing the Surfaces of the Sphere Packs

After generating the sphere pack from PFC, it is necessary to triangulate the surfaces of those spheres and put them in a STereoLithography (STL) format as OpenFOAM, the software used to simulate Stokes equations accepts such structure. In the STL format, the normal unit vector plus the coordinates of the three vertices of each triangle that result from surface meshing the spheres in the porous medium are saved. Gmsh, which is a 3D finite element mesh generator with a built-in CAD engine [50] is a suitable tool which accomplishes the task. An example of surface meshing to a sphere pack is shown in Fig. 2-2. Gmsh is also capable of meshing the void spaces within the porous medium, however, the spheres in the medium are almost touching each other. In between such spheres, the volume needs a much finer mesh, otherwise issues in accuracy and convergence occur. The snappyHexMesh software, which is another mesh generator handles such issues better than Gmsh.

2.2.3 Meshing the Void-Space Within the Sphere Packs

Identifying the bounding container of the medium of interest is a necessary step in order to carry out pore-scale meshing. All the sphere packs that have been generated in this study fit a cubic box of volume $125mm^3$. The box, without the spheres in it, is meshed uniformly with 140 points in each of the x,y and z directions resulting in around 2.75 million hexahedral cells. This step is done via blockMesh, which is supplied with OpenFOAM [51]. BlockMesh is a basic meshing tool that is good for Cartesian grid generation. After that, snappyHexMesh, which is another meshing utility in OpenFOAM, takes the mesh generated from blockMesh, carves it and adjust it until it fits the geometry given in the STL file. This process reduces the total number of cells from 2.75 million to around 1 million. The meshes obtained from snappyHexMesh can be viewed in Fig. 2-3 and Fig. 2-4. It can be seen from both figures that there are holes connecting spheres that are adjacent to each other as if they are connected. It is very difficult to simulate flow quantities between two bodies that are very close to each as a much finer much is needed in the volumes close to the point of contact between such bodies. To overcome this, snappyHexMesh merges problematic regions, thus removing the difficulty. This scenario, where adjacent spheres are merged near the points of contact is realistic as grains' surfaces are degraded due to friction when they are in contact with each other. Most of the spheres that have been generated by PFC are close to their neighbors and a slight overlap at the contacts have been created by snappyHexMesh; thus the assumption that the porous media is composed of perfectly shaped spheres can be relaxed. In addition, the bounding box of the host medium has been tightened to cross a portion of the boundary spheres as this eliminates the creation of a void space outside the porous medium which favors flow through some channels over others. In the meshing process, blockMesh takes a few seconds to run while snappyHexMesh takes around 20 minutes to complete the chiseling process.

a

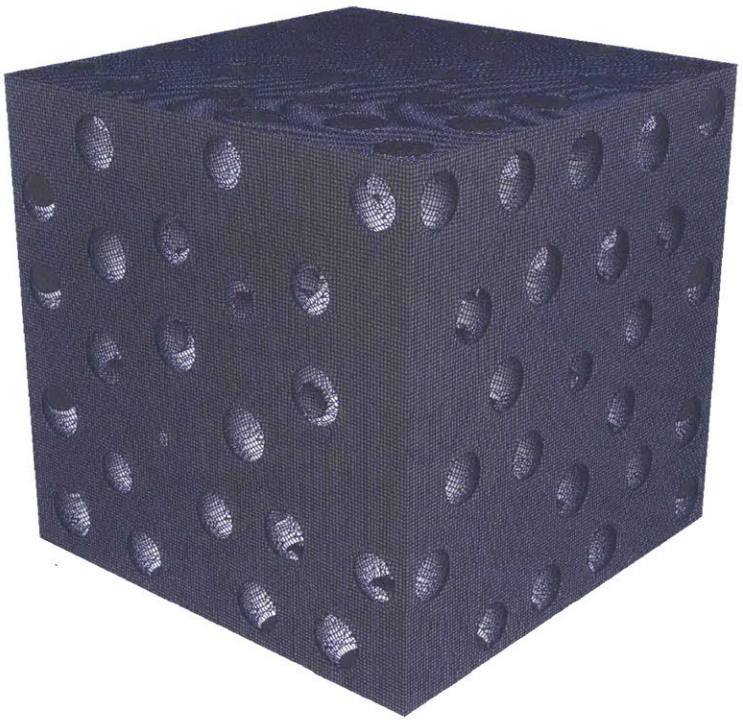

b

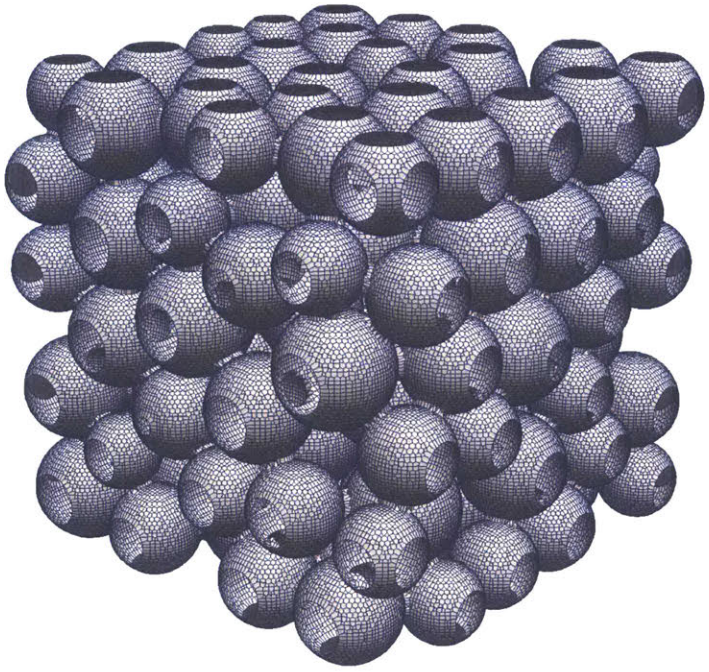

Figure 2-3: (a) View of the mesh generated by snappyHexMesh at the bounding box of a 3D porous medium, (b) View of the internal portion of the same medium with the outline at their surfaces being are faces of volume elements that belong to the volumetric mesh of the pore-space.

a

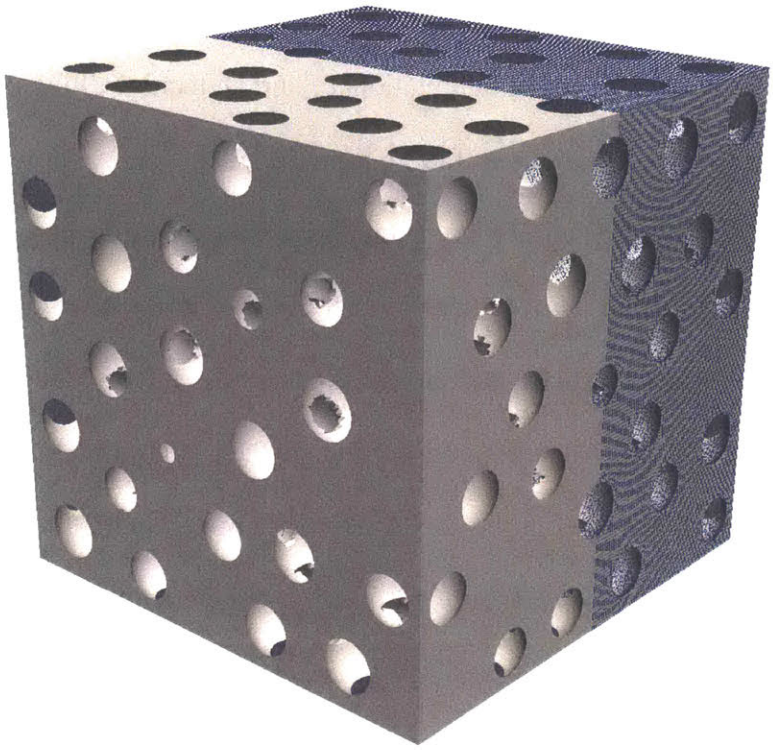

b

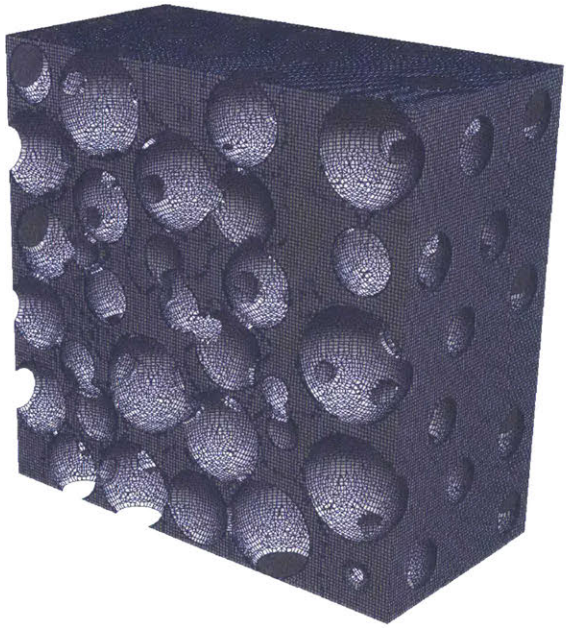

Figure 2-4: (a) View of the mesh generated by snappyHexMesh at the bounding box of a 3D porous medium with an outline of the grey part that has been discarded in (b), (b) View of the mesh inside of the same 3D porous medium with a portion of it being clipped.

2.2.4 Solving Stokes Equations at the Void-Space within the Spherical Packs

OpenFOAM, which is an open-source Computational Fluid Dynamic (CFD) software [51] is used in this work to solve Stokes equations at the void-space left by the sphere packs. OpenFOAM solves Stokes problem via the SIMPLE algorithm, which has been developed by Spalding and Patanker [52,53]. This algorithm is executed in OpenFOAM via the command simpleFoam. An alternative approach to solve Stokes equations is using the solver icoFoam that solves the incompressible laminar Navier-Stokes equations using the PISO algorithm that has been developed by Ferziger and Peric [54]. We modify the solver internally by removing the non-linear advection term from Navier-Stokes equations and solving Eq.(2.1) along with the following transient version of Stokes equations until steady state is reached where the derivative of velocity with respect to time vanishes.

$$\frac{\partial \boldsymbol{u}}{\partial t} + \mu \nabla^2 \boldsymbol{u} = \nabla p \tag{2.6}$$

Since Eq. (2.6) is transient, zero velocity and pressure are set as initial conditions at the void-space in the sphere pack. In the simulations, the time increment Δt is set to be 10^{-8} seconds, which was found to be a stable with our set-up that composes of 1 million computational grids occupied in a 125mm^3 container and a dynamic viscosity μ which has been set up to $10^{-3} N\, s/m^2$. This choice of Δt yields to a Courant Number, $C_o \ll 1$ at each time step, which is defined as

$$C_o = \Delta t \sup_{i \in \Omega} \left(\frac{u_{x,i}}{\Delta x_i} + \frac{u_{y,i}}{\Delta y_i} + \frac{u_{z,i}}{\Delta z_i} \right) \tag{2.7}$$

Here, Ω is the computational domain, which is the void-space in the porous medium, i is the grid number, $\boldsymbol{u}_i = (u_{x,i}, u_{y,i}, u_{z,i})$ is the velocity vector at cell i and $\boldsymbol{\Delta}_i = (\Delta x_i, \Delta y_i, \Delta z_i)$ is average element size vector in the same cell. The significance of C_o is that it tells us how fluid particles move from one cell to another in the computational domain. For instance, $C_o \leq 1$ means that in a single time step, a fluid parcel, at most, moves from one cell to a single adjacent cell. On the other hand, $C_o > 1$ implies that a single fluid particle moves through two or more cells in a single time step. For problems which involve flow in porous media where it takes time for a fluid particle to flow from one point to another, Courant number C_o is expected to be much smaller than 1 at every time step in order for simulations to run accurately without convergence issues.

2.2.5 Visualizing and Post Processing of Results

After reaching steady state and obtaining flow quantities (velocity field $\boldsymbol{u}$ and pressure p) that solve Stokes equations at the spaces between the rigid spheres, ParaView [55] is used to visualize these quantities everywhere in the 3D porous medium. ParaView is an open-source application that is capable of performing data analysis and scientific visualization. It is also capable of cutting surfaces of arbitrary shape, extracting and visualizing data at those surfaces. Examples of what the software is capable of doing are shown in Fig. 2-6 and Fig. 2-7, which show the three components of the velocity field, along with the velocity magnitude at a 2D slice parallel to both the inlet and outlet. ParaView, which uses a Python interface to run batches, is compatible with OpenFOAM and can be executed simply via the command paraFoam. However, OpenFOAM results should be first converted into Visualization Toolkit (VTK) format before using ParaView. To do this, the command foamToVTK is executed in the OpenFOAM directory where the desired results ($\boldsymbol{u}$ and p) exist before executing the command paraFoam.

a

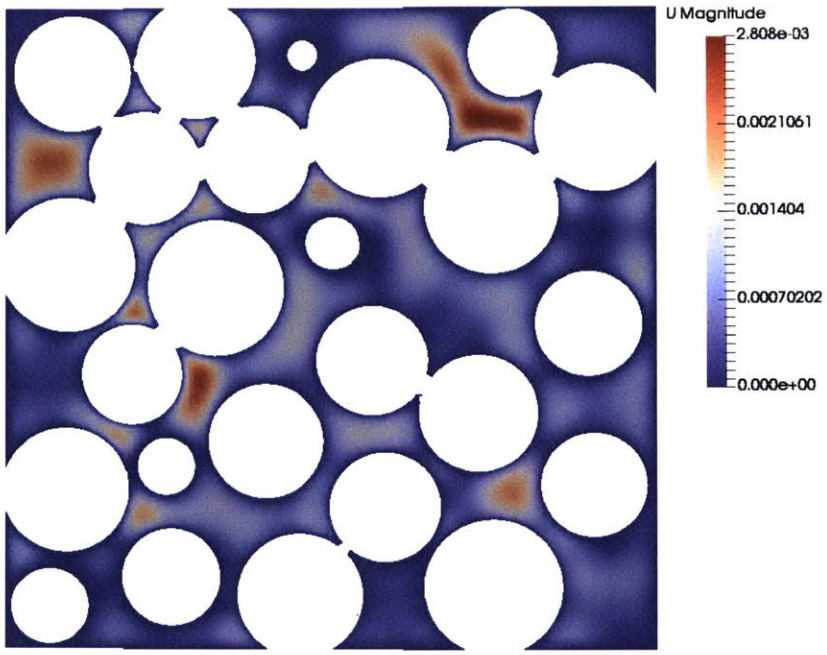

b

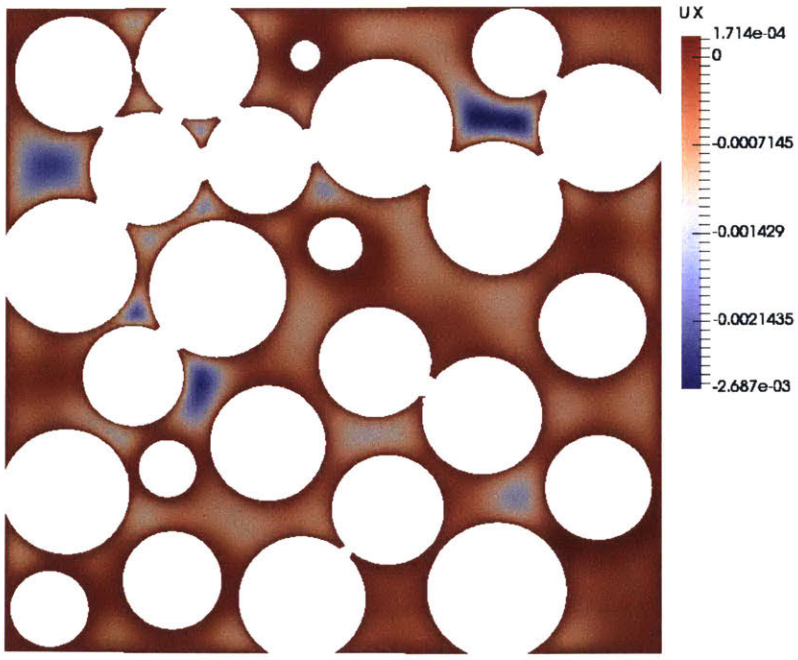

Figure 2-5: (a) View of the velocity magnitude at a 2D slice parallel to the inlet and outlet that is obtained from solving Stokes equations with $\mu = 10^{-3} N\, s/m^2$, (b) The same figure as (a) but shows the magnitude of the x-component of the velocity only.

a

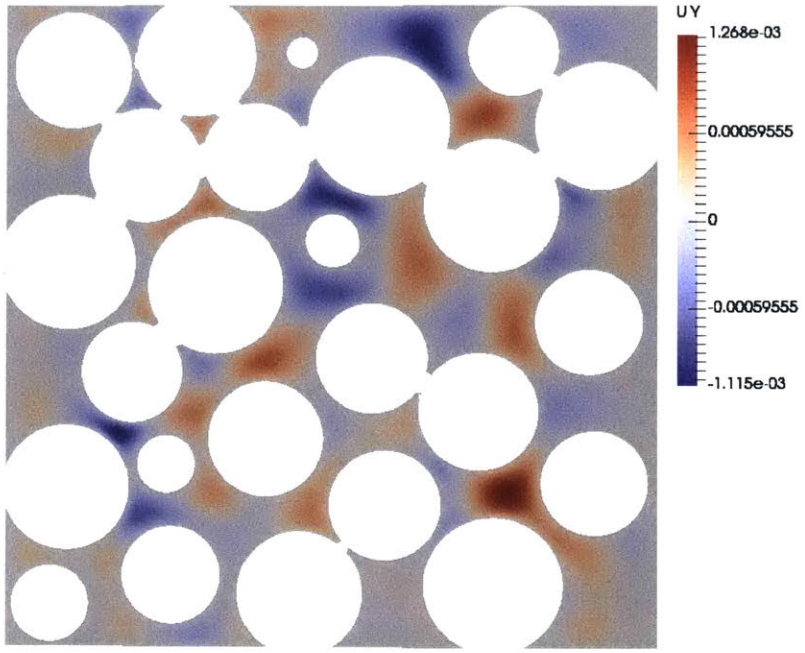

b

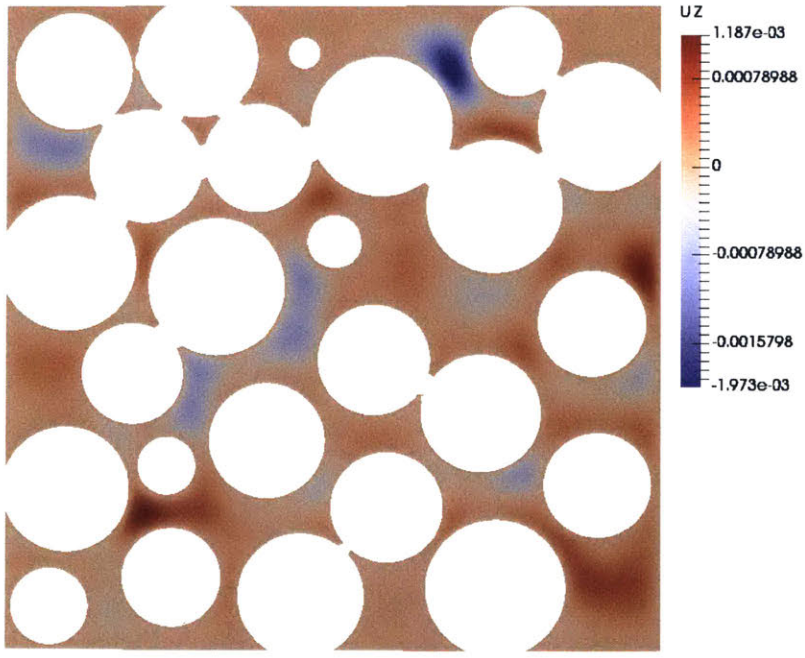

Figure 2-6: (a) View of the y-component of the velocity at a 2D slice parallel to the inlet and outlet that is obtained from solving Stokes equations with $\mu = 10^{-3} N\ s/m^2$, (b) The same figure as (a) but shows the magnitude of the z-component of the velocity only.

Chapter 3

Results and Discussion: Analysis of the Velocity Distribution from Solving Stokes Equations

3.1 Simulation Results of Stokes Equations

3.1.1 Computational Domain

In a 3D porous medium composed of a dense sphere pack and contained in a cubic box of volume 125mm^3, the void space has been discretized with approximately 1 million hexahedral cells. Simulations of the transient version of Stokes equations have been set to end at time 4×10^{-4} seconds where steady-state is reached to Eq. 2.6 within an accuracy of 6 digits. The time increment Δt is fixed to 10^{-8} seconds. In a workstation with an Intel Core i7 2.6GHz CPU, and 16GB memory, a total time of 3 days is needed to complete the 40,000 time-steps in order for steady flow to occur. The dynamic viscosity μ has been chosen to be $10^{-3}\ N\ s/m^2$; however, this quantity can be set arbitrarily as it vanishes after $\boldsymbol{u}$ is rescaled to its mean value. Twelve sphere packs have been generated, where the distribution of the squared radius of the spheres in m^2 for the first five packages range from 1.4×10^{-7} to 3.2×10^{-7}, for the next three packs the range is a bit wider, to become 1×10^{-7} to 3.2×10^{-7}, while for the last four packs the lower bound increases and the range becomes 2×10^{-7} to 3.2×10^{-7}. The upper bound for the squared radius of the spheres has been fixed for all the twelve sphere packs while the lower bound has been varied. The porous media have been generated so that they are contained in a cubic box to reduce the effect of edges on flow patterns.

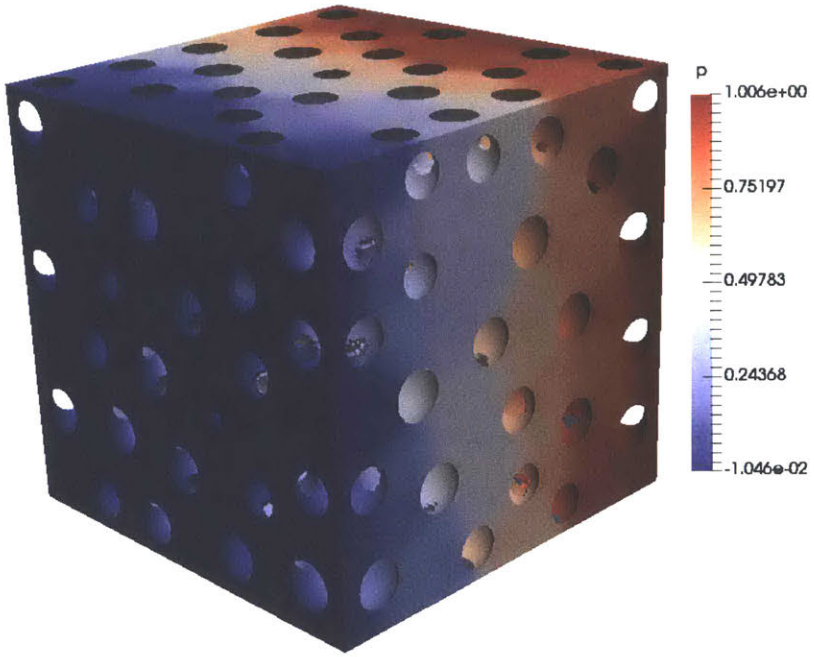

Figure 3-1: Visualization of the pressure that resulted from solving Stokes equations at the outer box of a 3D porous medium composed of random and dense sphere pack.

3.1.2 Pressure Field

After solving Stokes equations with the boundary conditions in Eq. 2.3-2.5, where the pressure is set to be 1 at the inlet (the back side of the box) and 0 at the outlet (the front side of the box), the pressure at the bounding box is visualized in Fig. 3-1. Regards to the pressure in the void-spaces between the spheres, for a typical 2D slice parallel to both the inlet and outlet, the pressure does not vary significantly between points on the slice compared to other points far away from the slice. This is evident from Fig. 3-1 where the pressure scale (color) at the top and front sides of the box can be seen as connected strips parallel to both the inlet and outlet's top and side boundaries. Also, for a typical 2D slice perpendicular to both the inlet and the outlet, the pressure decreases somewhat linearly from the inlet to the outlet, except in the regions close to the spheres, where the pressure does not vary significantly there. Therefore, pressure variation in 3D porous media driven by a single pressure gradient is predictable and will not be a focus of this thesis.

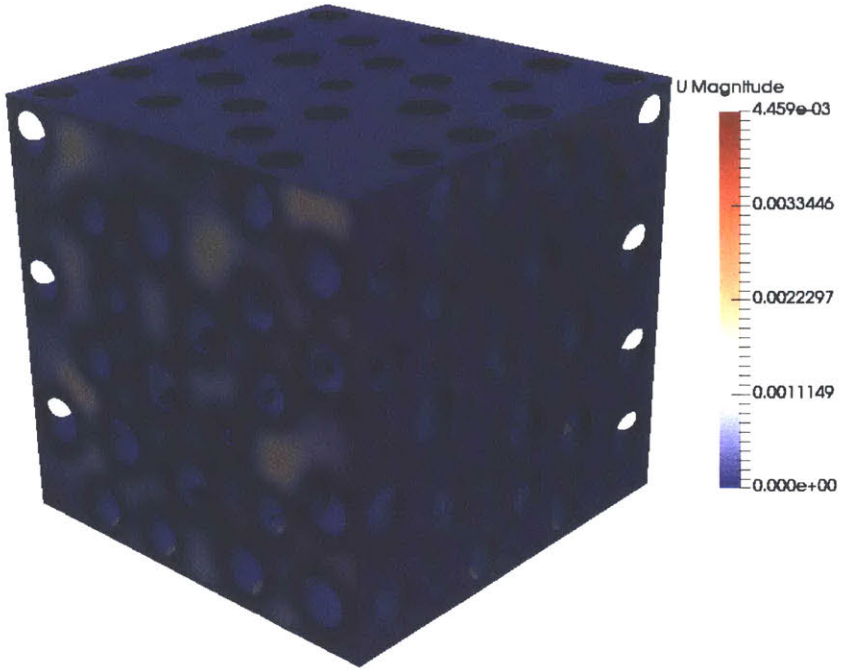

Figure 3-2: Visualization of the velocity magnitude that resulted from solving Stokes equations at the outer box of a 3D porous medium composed of random and dense sphere pack.

3.1.3 Velocity Field

Visualization of the velocity magnitude at the bounding box of a 3D porous media is shown in Fig. 3-2. At the inlet and outlet, the tangential component of the velocity has been set to zero while zero velocity, which is the no-slip boundary condition, has been imposed at the other 4 faces of the box. In addition, 2D views of the velocity's components plus magnitude at a slice parallel to both the inlet and outlet are shown in Fig. 2-5-and 2-6. Unlike pressure, the velocity magnitude varies in the void spaces significantly depending on the geometry of the host medium. Distinct behaviors for high and low velocities have been established by both computational [19, 41, 42, 44, 45] and experimental [36, 37, 40] studies. It has been concluded that high velocities are controlled by the formation of channels, while low velocities are dominated by stagnation zones. Predicting the exact locations of both high and low velocities in a 3D porous medium is a difficult problem that has not been established yet; however, the focus here is studying the velocity distribution.

3.2 Velocity Distribution in 3D Porous Media

3.2.1 Probability Distribution Fitting

Let U be the set of all velocity magnitudes in the computational grids at the void-spaces in a 3D porous medium that has been obtained from solving Stokes equations (Eq. 2.1-2.2) with the boundary conditions (Eq. 2.3-2.5). We denote $\langle U \rangle$ to be the average value of the quantities in the set U and $U_r = U/\langle U \rangle$ be the set of all velocity magnitudes at the same void spaces rescaled by their mean value. The volumes of the computational cells in the porous media are assumed to be approximately the same, which is a reasonable assumption, as a uniform grid has been generated by blockMesh before snappyHexMesh chisels the mesh to fit the spheres, as discussed in section 2.2. In this study, it has been found that the probability density function (PDF) of U, for all the twelve sphere packs with different ranges of the squared radius of the spheres, has a Gamma distribution. With a shape parameter $k > 0$ and a scale parameter $\theta > 0$ such that $U \sim \text{Gamma}(k, \theta)$, the following relations hold:

$$f_U(u) = \frac{1}{\Gamma(k)\theta^k} u^{k-1} e^{-u/\theta}, \quad u \in (0, \infty) \tag{3.1}$$

$$cU \sim \text{Gamma}(k, c\theta), \quad c > 0 \text{ is a scalar} \tag{3.2}$$

$$\langle U \rangle = k\theta \tag{3.3}$$

From Eq. 3.2-3.3, it can be easily deduced that $U_r \sim \text{Gamma}(k, 1/k)$. Plots of the PDF of U_r for one sphere pack, along with the Gamma distribution that best fit, both without and with a log-log scale of the axes, are shown in Fig. 3-3. In addition, Table 3-1 gives the values of k in the Gamma distribution that best fit the PDF of U_r. For all the twelve 3D porous media composed of spheres, $k \approx 1.05$ and $\text{Gamma}(k, 1/k)$ has a mean value of 1.

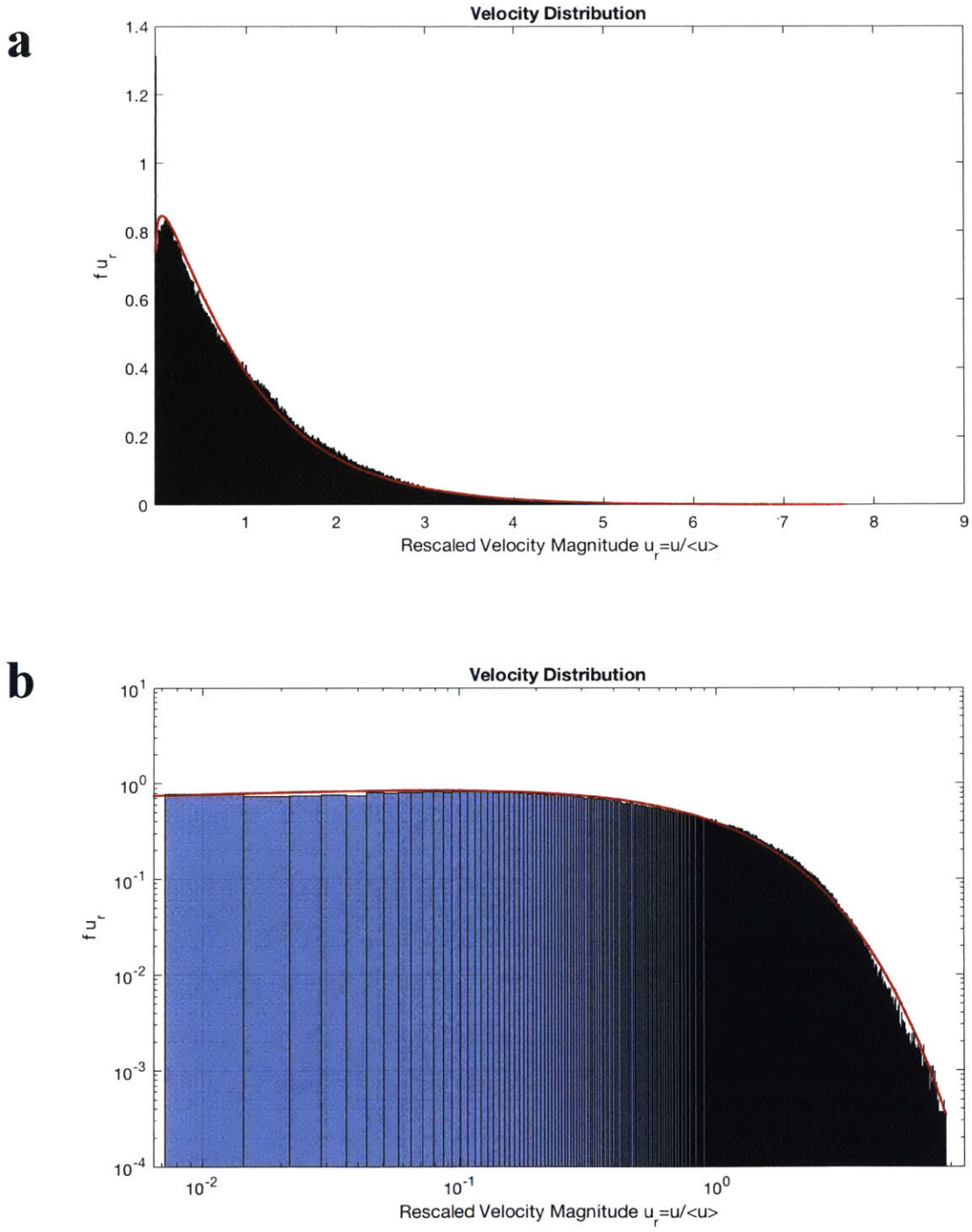

Figure 3-3: (a) Plot of the PDF of the rescaled velocity magnitudes U_r at the void-spaces in a 3D porous medium that has been obtained from solving Stokes equations. (b) Same plot as (a) but in log-log scale. The red plot is the Gamma distribution with shape parameter that fit the PDF of U_r.

Table 3-1: The values of the shape parameter k in the Gamma distribution that best fit the PDF of the rescaled velocity distribution for each of the twelve sphere packages.

Package number	k
1	1.059
2	1.049
3	1.082
4	1.026
5	1.063
6	1.099
7	1.103
8	1.082
9	1.040
10	1.034
11	1.072
12	1.076

3.2.2 The Distribution of Low Velocities

From Fig. 3-3(b), it can be seen that for low velocities that are far away from the mean, a line of slope almost zero fits the PDF of U_r, when it is displayed in log-log format. This behavior has been observed in all sphere packs and can be explained by studying the slope of the PDF of $\log U_r$. With $V = \log U_r$ where $U_r \sim \text{Gamma}(k, \theta)$ and $\theta = 1/k$, the PDF of V is shown below

$$f_V(v) = e^v f_{U_r}(e^v) = \frac{1}{\Gamma(k)\theta^k} e^{vk - e^v/\theta} \tag{3.4}$$

$$\frac{df_V(v)}{dv} = \frac{k - \zeta}{\Gamma(k)} \zeta^k e^{-\zeta}, \quad \zeta = \frac{e^v}{\theta} \tag{3.5}$$

Assume that v is far away from the mean, that is $v \ll 0$. It is easy to see that $df_V(v)/dv > 0$ for all $v < 0$. Imposing $v \ll 0$ or equivalently $\zeta \to 0$ implies $df_V(v)/dv \to 0$ as $(k - \zeta)e^{-\zeta}$ in the expression of the derivative is bounded above by k which leaves the term ζ^k that goes to 0.

3.2.3 Linking Velocity Distribution with the Statistics of Pore-Structures

From the previous two sections, we have seen that $U_r \sim \text{Gamma}(k, 1/k)$ which has a mean value of 1 and that the PDF of $\log U_r$ can be fit by a straight horizontal line for low velocities far away from the mean. For high velocities, the log-Gamma distribution does not fit the PDF of $\log U_r$ well. Therefore, for low velocities that are much smaller than the mean, which is the focus region, the behavior of the PDF of $\log U_r$ can be predicted with a reasonable approximation to k. Therefore, to have a good fit for low velocities, it is sufficient to find a parameter, which characterizes the geometry of the host medium, that correlates well with k. For the twelve sphere packs that have been generated, the correlation coefficient between k and the mean, standard deviation and the coefficient of variation of the spheres' radii, surface area and volumes have been computed. However, the volume fraction of the porous media for the twelve packages has been found to connect well with the shape parameter k obtained in Table 3-1. Despite the fact that an empirical relation that links k with the statistics of the pore-structure is not necessarily unique, the volume fraction $1 - \phi$, where ϕ is the porosity of the host medium is chosen to be linked with k. Porosity is the fraction of the volume of open spaces in a 3D porous medium over the total volume of the bounding box that contains the spheres. For a cubic packing arrangement of spheres, porosity is about 0.47 for a typical pack. In our generated packs with an arrangement that is comparable to cubic, porosity varies from 0.4321 to 0.4576. Such range of porosity, despite being narrow, is typical for a dense sphere pack contained in a cubic box. With a Pearson-correlation coefficient between k and $1 - \phi$ of 0.7171, which indicates a strong linear relationship between these two quantities and setting $k = 1.98(1 - \phi)$ which is the best linear fit, the predicted value of the PDF of U_r is given by

$$U_r^{predit} \sim \text{Gamma}\left(1.98(1-\phi), \frac{1}{1.98(1-\phi)}\right) \tag{3.6}$$

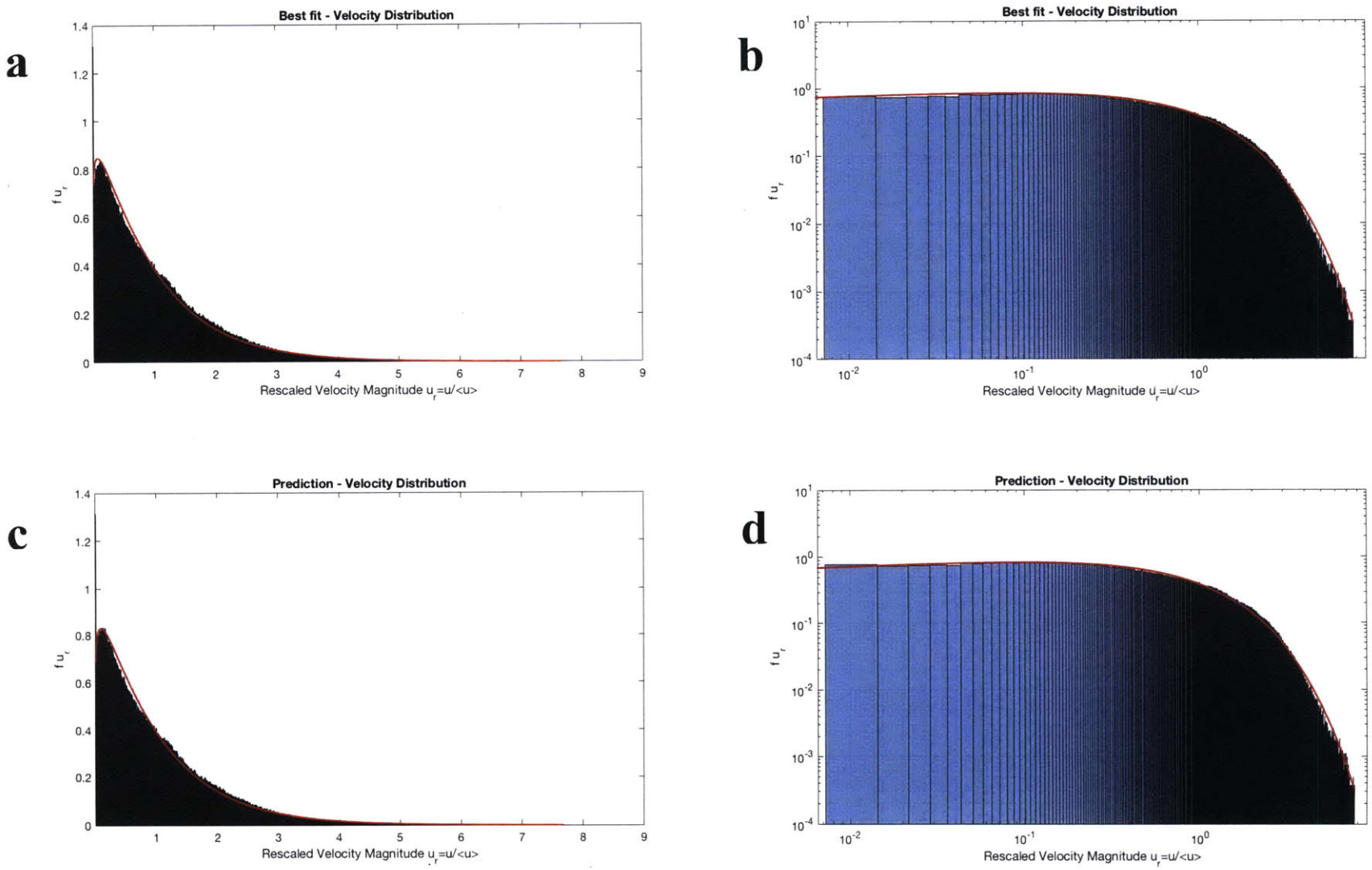

Figure 3-4: (a) Plot of the PDF of the rescaled velocity magnitudes U_r at the void-spaces in a 3D porous medium that have been obtained from solving Stokes equations. (b) The same plot as (a) but in log-log scale. The red plot is the Gamma distribution with shape parameter that fit the PDF of U_r. In (c) and (d), the Gamma distribution with predicted k has been used.

Fig. 3-4 shows a comparison between the shape parameter k in the Gamma distribution that best fit the PDF of U_r along with a plot of the relation in Eq. 3.6 on top of the PDF of U_r . Similar plots for all of the twelve sphere packs are shown in the Appendix. Despite a simple predictive relation, Eq. 3.6 performs well for all packs. To predict the distribution of the magnitude of velocities without rescaling at the empty spaces in the porous medium $U \sim \text{Gamma}(k, \theta)$, it is only needed to predict $\theta = \langle U \rangle / k$ or equivalently predict the value of the mean velocity $\langle U \rangle$ accurately. This can be done via Darcy's law that is shown below

$$\langle U \rangle = \frac{\Delta P}{L} \frac{\kappa}{\mu} \tag{3.7}$$

Here, ΔP is the pressure drop across the porous medium, L is the length of the bounding cubic box that bound the spheres, μ is the dynamic viscosity of the fluid and κ is the permeability of the porous medium. The permeability in 3D porous media with sphere packing can be calculated using the approach in [56] where a data-driven framework of the host medium has been used to analyze fluid flow and calculate permeability, which has been verified to scale well with the average pore-void ratio and the average pore network closeness centrality. Studying permeability in porous media is out of the scope of this thesis and is a topic of its own; however, accurate computation of κ implies the ability to predict θ and $U \sim \text{Gamma}(k, \theta)$.

Chapter 4

Conclusions and Open Questions

4.1 Conclusions

In this thesis, we have studied flow in random dense spherical packs. We have described the software architecture used to perform high-resolution simulations of Stokes equations; from the generation process of the sphere packs to the meshing procedures and massaging data format all the way to visualization of simulation results. We have simulated flow at low Reynolds numbers by solving the Stokes equations with the finite volume method and imposing a no-slip boundary condition at the boundary of each sphere. High fidelity numerical simulations of Stokes flow have been performed using OpenFOAM. Visualization of both the velocity fields and the pressure in the generated media have been included in this thesis along with the probability density function (PDF) of the rescaled velocity magnitudes in the host media. We have shown that the distribution of low velocities in 3D porous media is described well by a Gamma distribution, which is robust to variations in the geometry of the porous media. We have developed a simple model that predicts the parameters of the gamma distribution in terms of the porosity of the host medium. Despite its simplicity, the predictions from our model agree well with high-resolution simulations in terms of the velocity distribution. We have shown that for low velocities that are far away from the mean, a straight line of slope zero fits the PDF of the logarithm of the rescaled velocities Within the confines of relatively homogeneous spherical bead packs, our results indicate that the full fluid velocity distribution can be predicted directly from the porosity of the bead pack.

4.2 Open Questions and Challenges

It is known that the behavior of velocities in porous media is influenced directly by the pore structure; that is, the open space left by the solid fraction in the host medium. However, it is not clear why the velocity distribution for single-phase laminar flow in a random dense sphere pack has a Gamma distribution, which is a well-structured behavior that arises consistently despite randomness in the generated geometry. A similar distribution has been seen in mixing problems [57] in which the nature of their tackled problem and setup differ significantly from ours. The theoretical justification of this observation, despite being challenging to obtain, can give us insight into how different flow problems can be linked to one another. It will be interesting to investigate flow through porous media composed of non-spherical packs and see whether similar distributions carry over to a more complex setup. In this study, the focus was on low velocities and it is worth studying the distribution of high velocities and figure out what determines their distribution. Are the channels with minimum resistance control high-velocity distributions in porous media? Is flow in a complex porous medium equivalent to flow with similar complexity in a simpler medium? It is worthy increasing the complexity of the system by studying flow in media with fractures as well.

In addition, the work presented in this thesis can be extended to the multiphase case in which the solution of (multiphase) Stokes flow equations in complex 3D geometries (such as granular packs or rough fractures), coupled with transport solvers for passive particles or phase fields can be analyzed. Nevertheless, in multiphase flow, the difficulty of predicting flow quantities from the statistics of pore structures escalates drastically and vary significantly depending on wetting properties and varying contact angles.

Appendix A

A.1 Velocity Distribution for All Generated Packs

Twelve dense sphere packs were generated via the software PFC, where each pack is contained in a cubic box of volume 125mm^3. The distribution of the squared radius r^2 of the spheres in meter square for the first five packages range from 1.4×10^{-7} to 3.2×10^{-7}. The range of r^2 for the next three packages is a bit wider, to become from 1×10^{-7} to 3.2×10^{-7}, while for the last four packs the lower bound increases and the range becomes 2×10^{-7} to 3.2×10^{-7}. The upper bound for the squared radius of the spheres has been fixed for all the twelve sphere packs while the lower bound has been varied.

The PDF of the rescaled velocity distribution $U_r \sim \text{Gamma}(k, 1/k)$ is plotted for all twelve sphere packs and is compared to the Gamma distribution with a shape parameter k that best fit the rescaled velocities. Also, another Gamma distribution with a predicted shape parameter $k = 1.98(1-\phi)$ is plotted on top of the PDF of U_r. From the figures (Fig. A-1 - A-12) shown in the following pages, (1) The distribution of low velocities in 3D porous media is described well by a Gamma distribution, which is robust to variations in the geometry of the porous media. (2) Our predictions (Eq. 3.6) agree well with high-resolution simulations in terms of the velocity distribution. (3) It is also clear that for low velocities that are far away from the mean, a straight line of slope zero fits the PDF of the logarithm of the rescaled velocities.

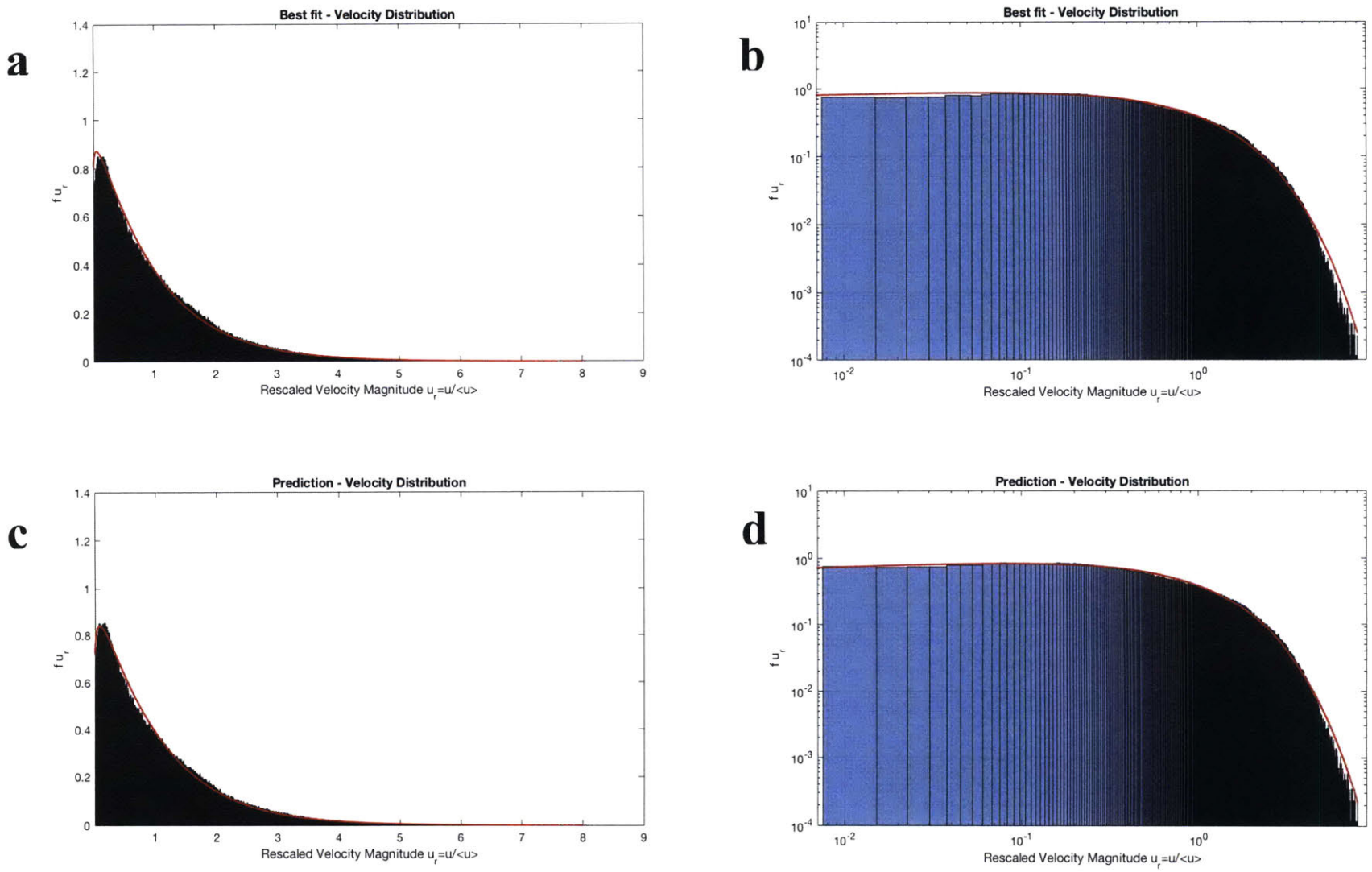

Figure A-1: For the 1st pack (a) Plot of the PDF of U_r (b) The same plot as (a) but in log-log scale. The red plot is the Gamma distribution with shape parameter that fit the PDF of U_r. In (c) and (d), the Gamma distribution with predicted value k has been used.

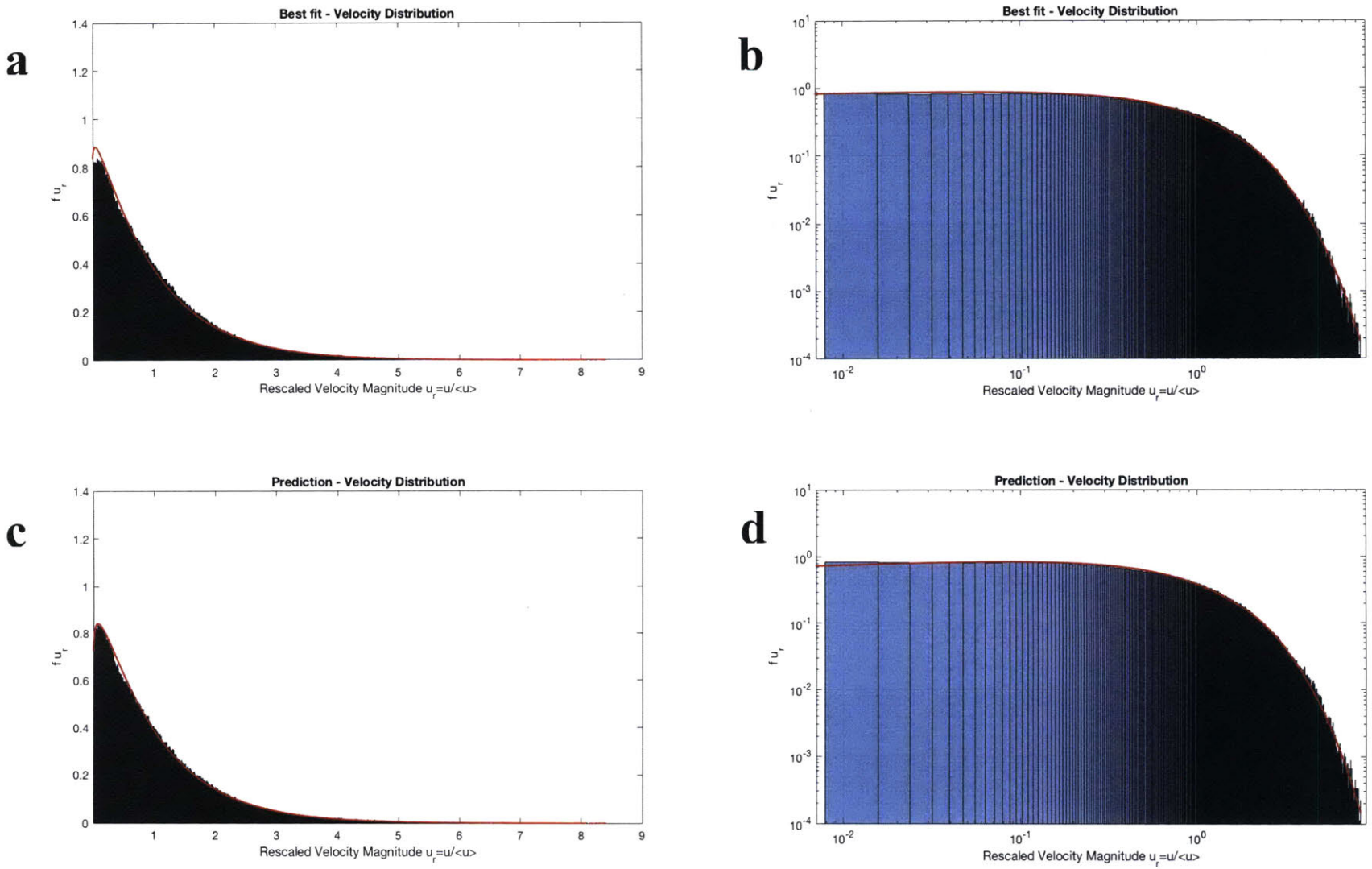

Figure A-2: For the 2nd pack (a) Plot of the PDF of U_r (b) The same plot as (a) but in log-log scale. The red plot is the Gamma distribution with shape parameter that fit the PDF of U_r. In (c) and (d), the Gamma distribution with predicted value k has been used.

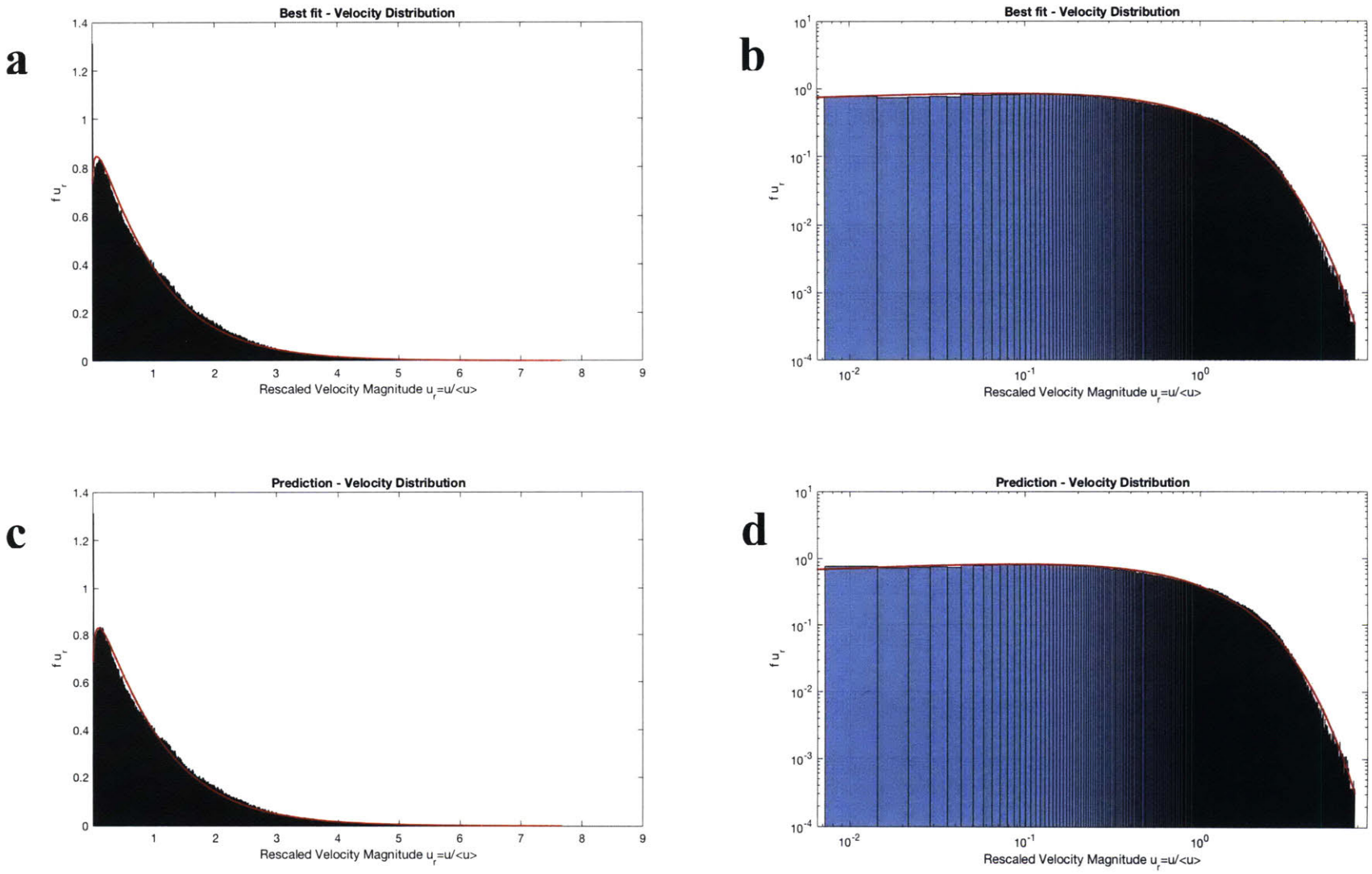

Figure A-3: For the 3rd pack (a) Plot of the PDF of U_r (b) The same plot as (a) but in log-log scale. The red plot is the Gamma distribution with shape parameter that fit the PDF of U_r. In (c) and (d), the Gamma distribution with predicted value k has been used.

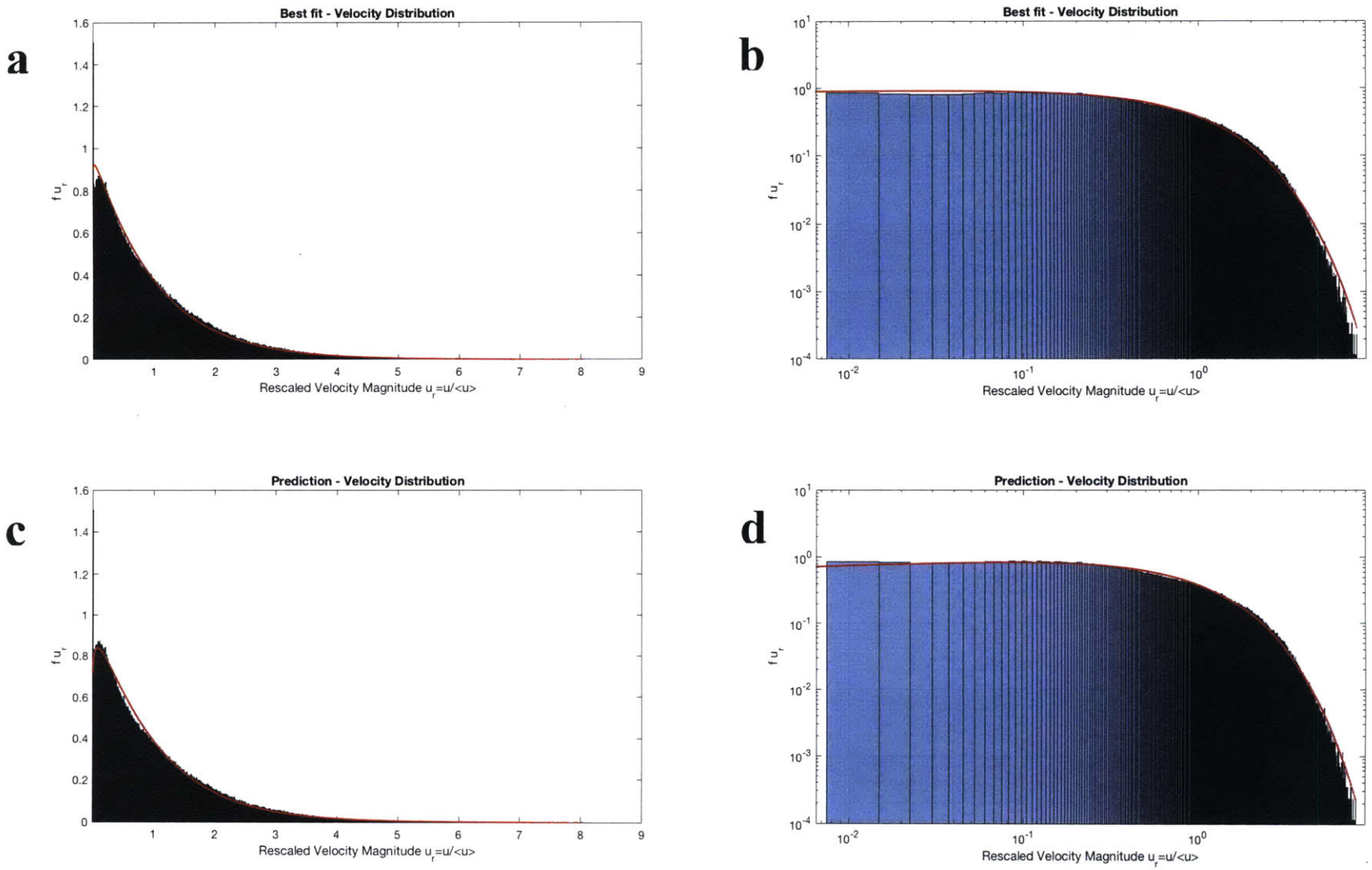

Figure A-4: For the 4th pack (a) Plot of the PDF of U_r (b) The same plot as (a) but in log-log scale. The red plot is the Gamma distribution with shape parameter that fit the PDF of U_r. In (c) and (d), the Gamma distribution with predicted value k has been used.

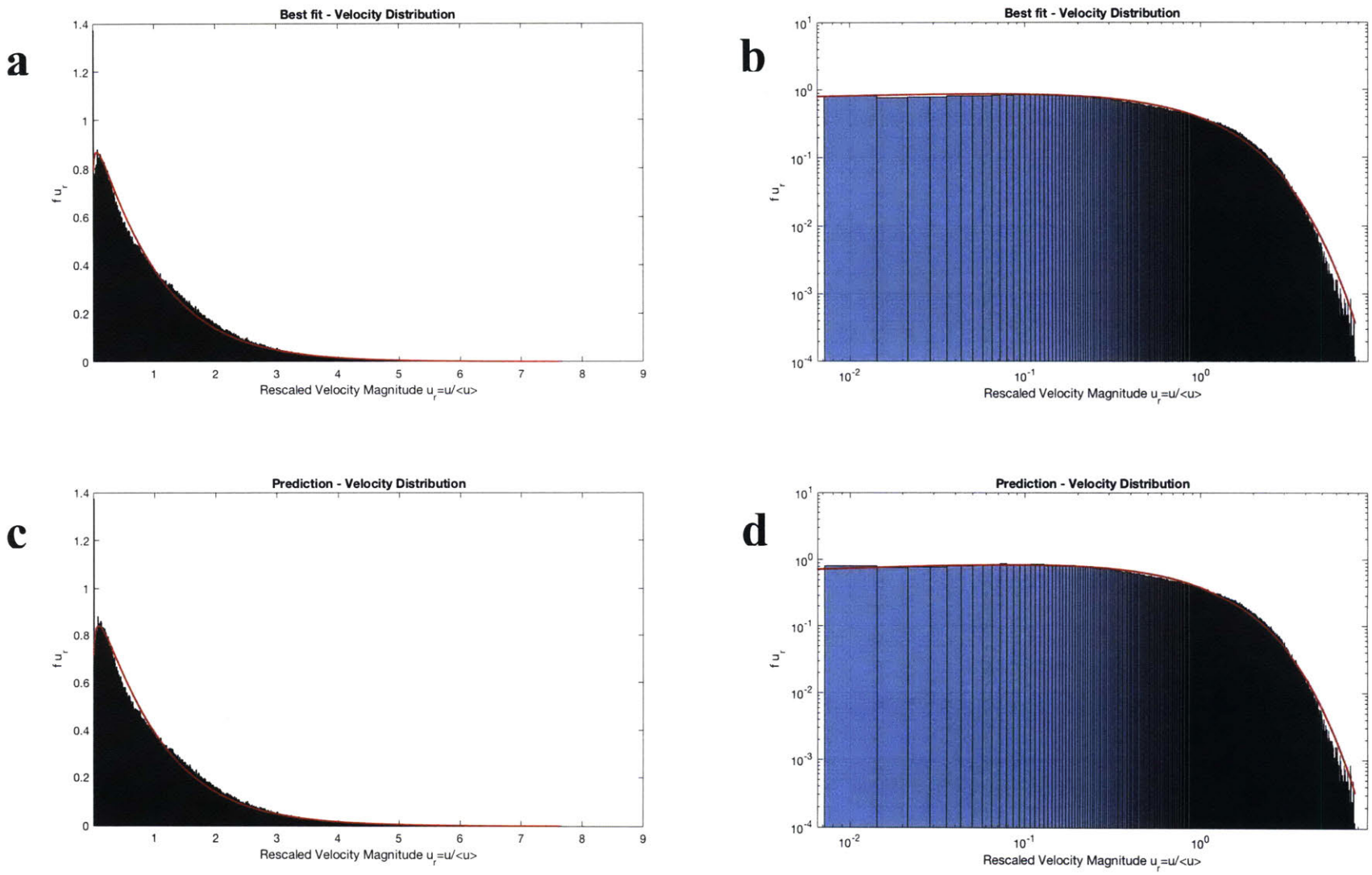

Figure A-5: For the 5th pack (a) Plot of the PDF of U_r (b) The same plot as (a) but in log-log scale. The red plot is the Gamma distribution with shape parameter that fit the PDF of U_r. In (c) and (d), the Gamma distribution with predicted value k has been used.

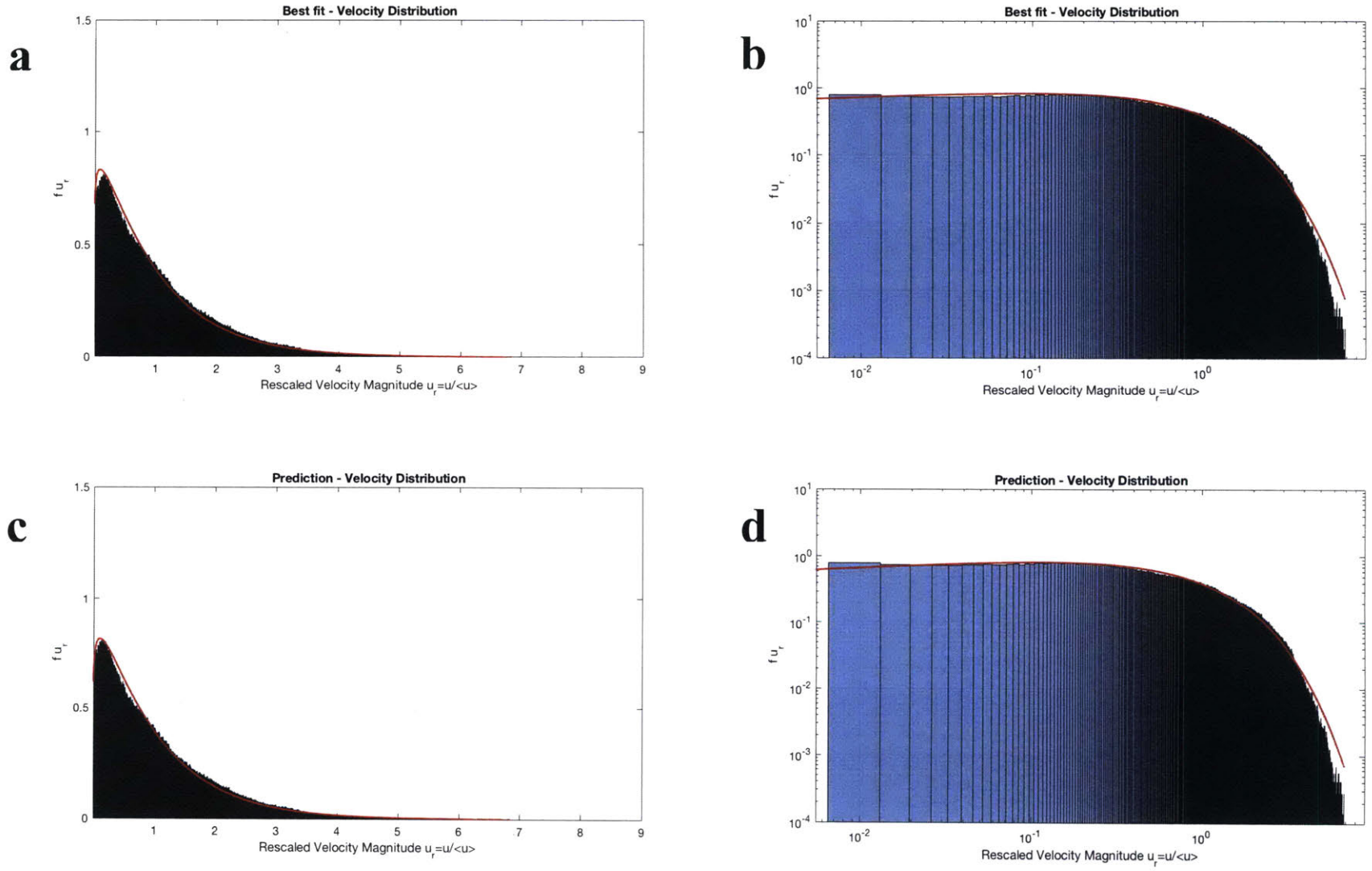

Figure A-6: For the 6th pack (a) Plot of the PDF of U_r (b) The same plot as (a) but in log-log scale. The red plot is the Gamma distribution with shape parameter that fit the PDF of U_r. In (c) and (d), the Gamma distribution with predicted value k has been used.

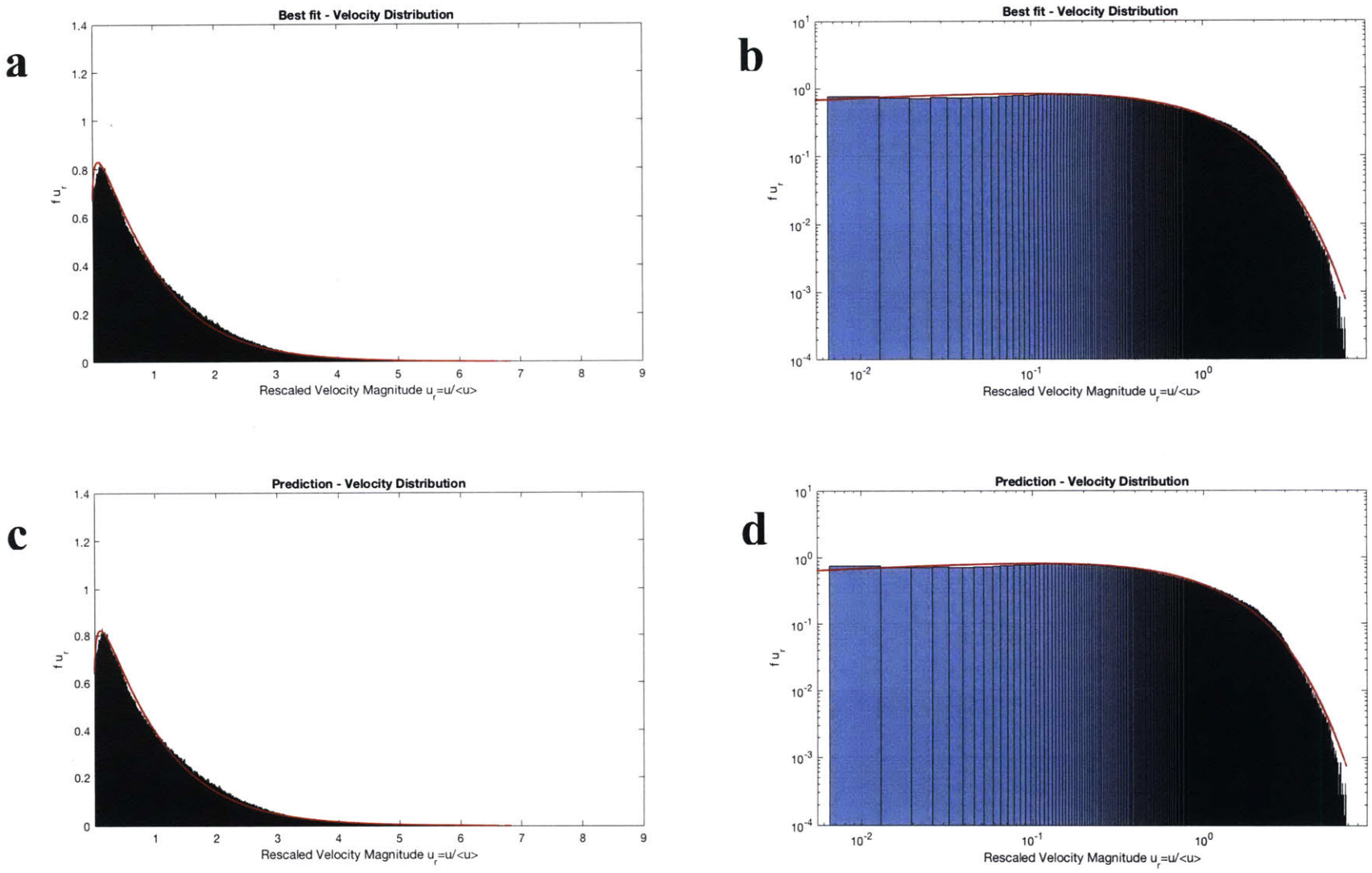

Figure A-7: For the 7th pack (a) Plot of the PDF of U_r (b) The same plot as (a) but in log-log scale. The red plot is the Gamma distribution with shape parameter that fit the PDF of U_r. In (c) and (d), the Gamma distribution with predicted value k has been used.

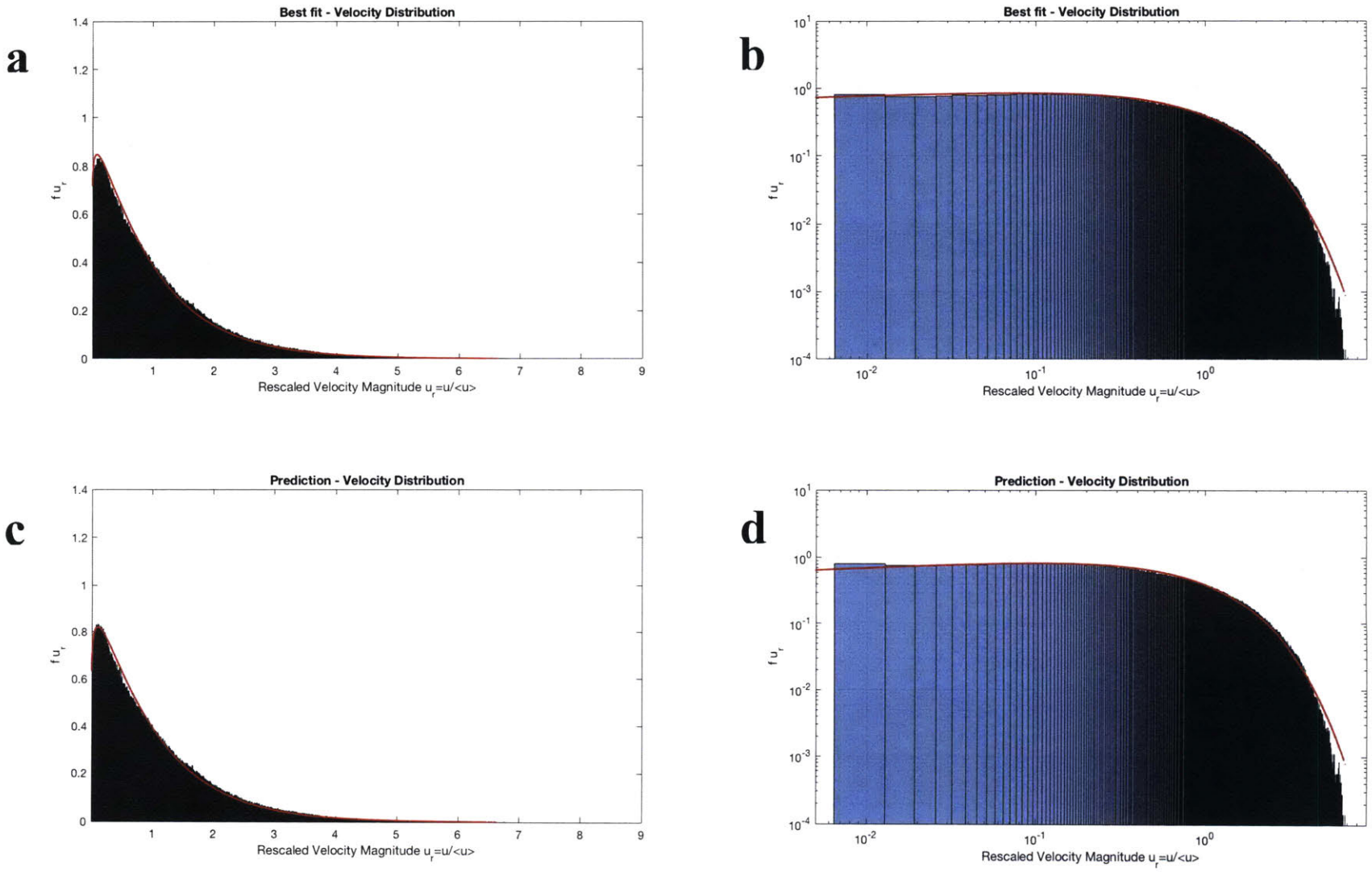

Figure A-8: For the 8th pack (a) Plot of the PDF of U_r (b) The same plot as (a) but in log-log scale. The red plot is the Gamma distribution with shape parameter that fit the PDF of U_r. In (c) and (d), the Gamma distribution with predicted value k has been used.

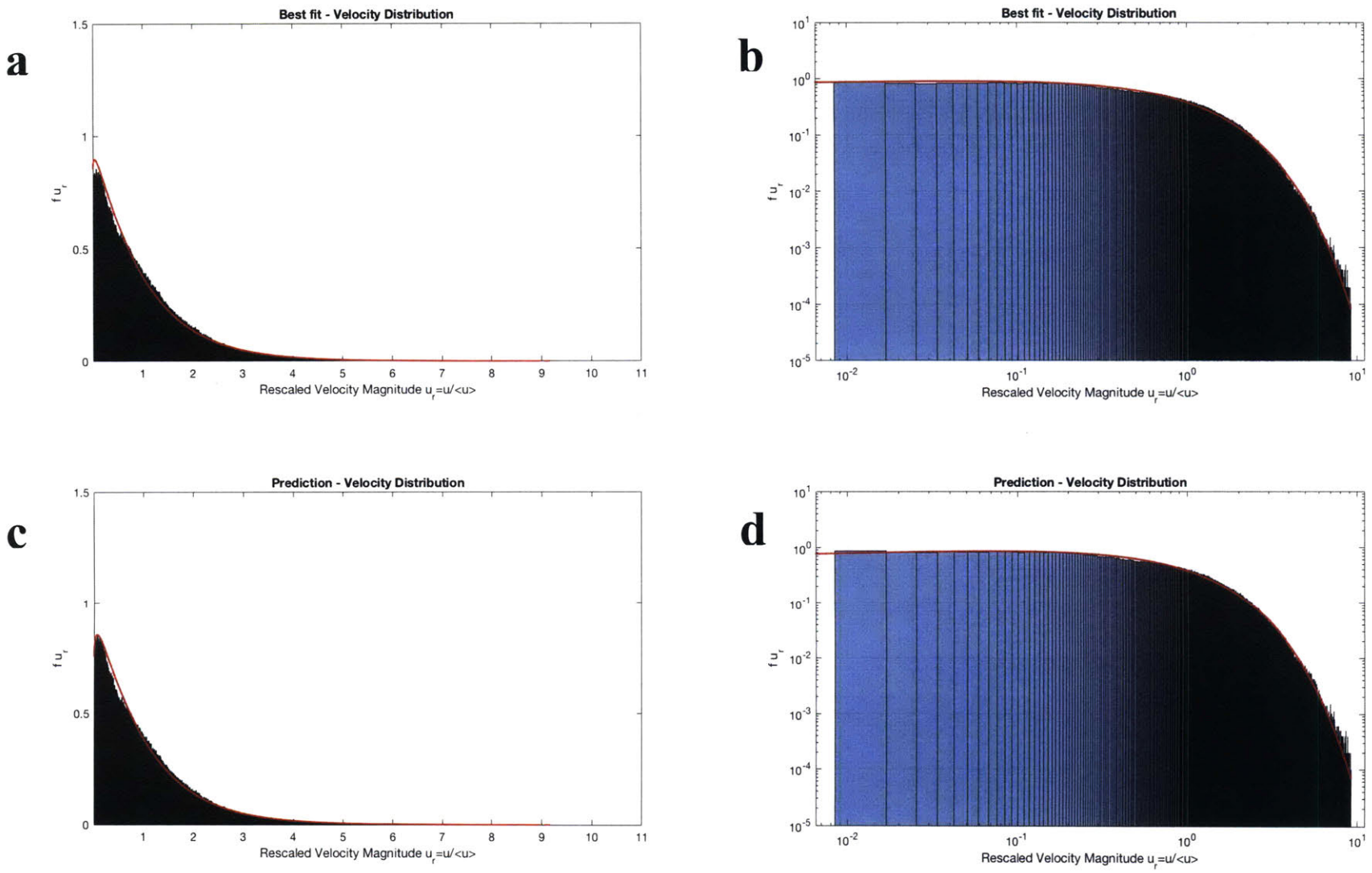

Figure A-9: For the 9th pack (a) Plot of the PDF of U_r (b) The same plot as (a) but in log-log scale. The red plot is the Gamma distribution with shape parameter that fit the PDF of U_r. In (c) and (d), the Gamma distribution with predicted value k has been used.

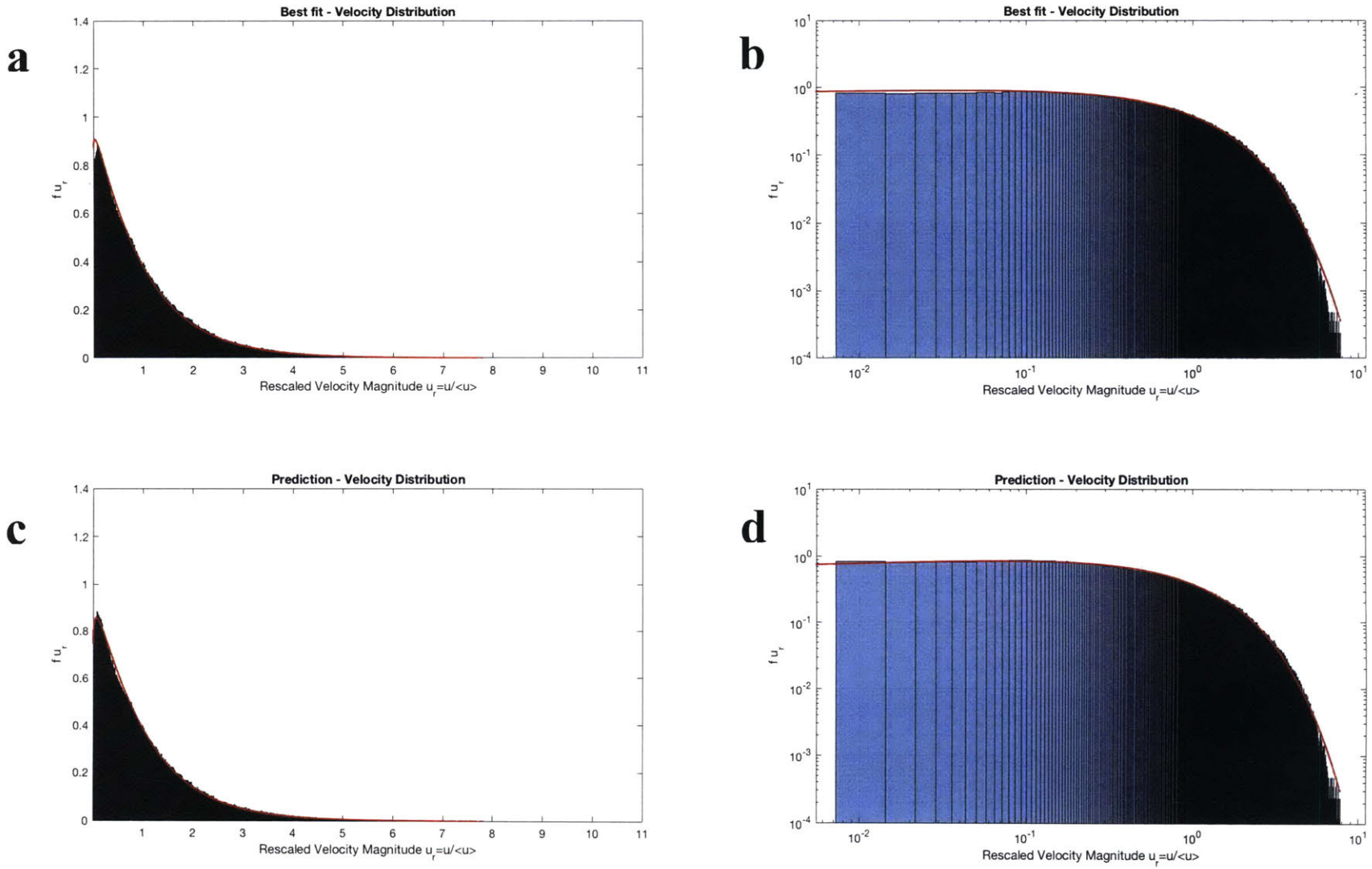

Figure A-10: For the 10th pack (a) Plot of the PDF of U_r (b) The same plot as (a) but in log-log scale. The red plot is the Gamma distribution with shape parameter that fit the PDF of U_r. In (c) and (d), the Gamma distribution with predicted value k has been used.

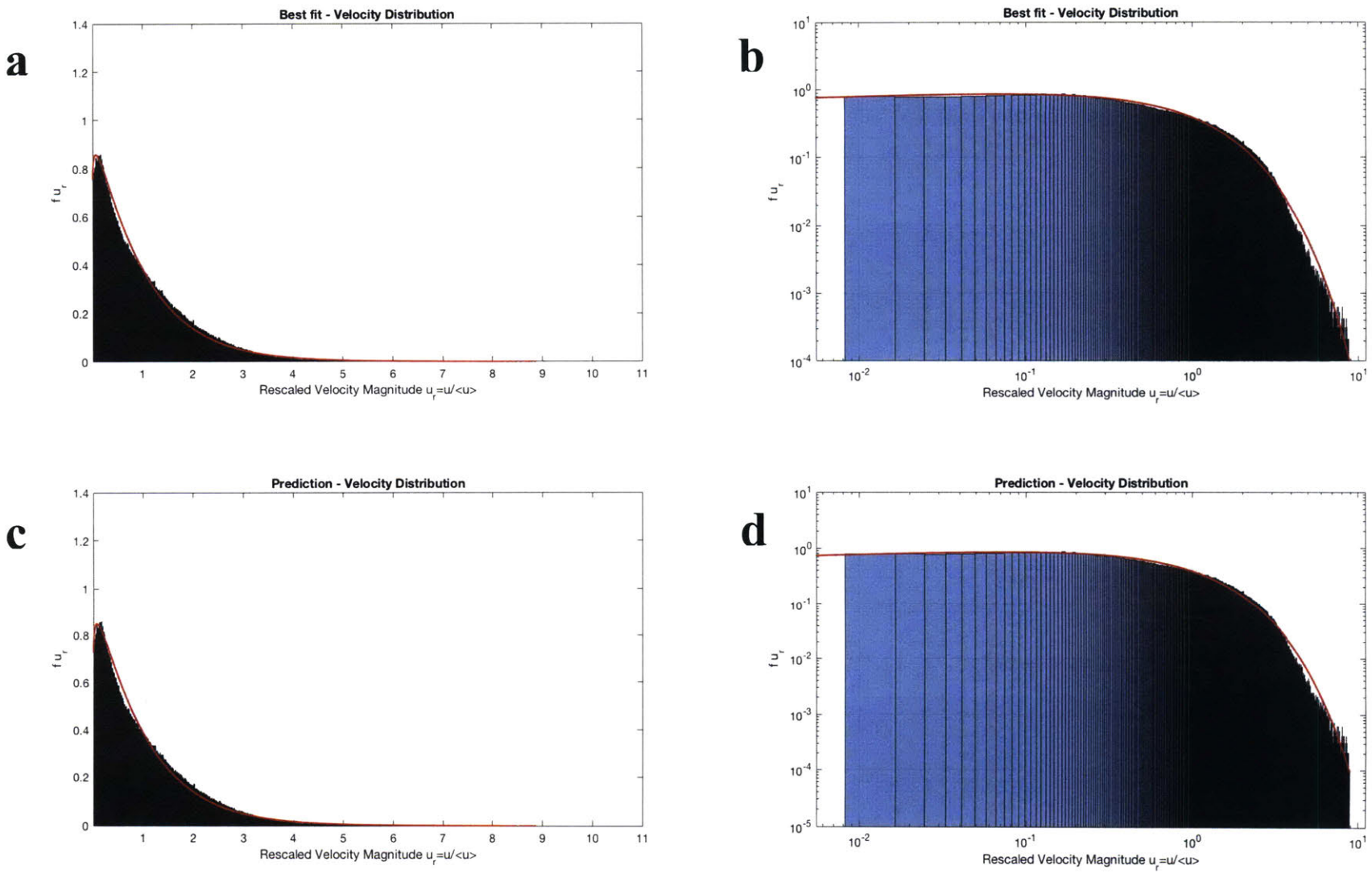

Figure A-11: For the 11th pack (a) Plot of the PDF of U_r (b) The same plot as (a) but in log-log scale. The red plot is the Gamma distribution with shape parameter that fit the PDF of U_r. In (c) and (d), the Gamma distribution with predicted value k has been used.

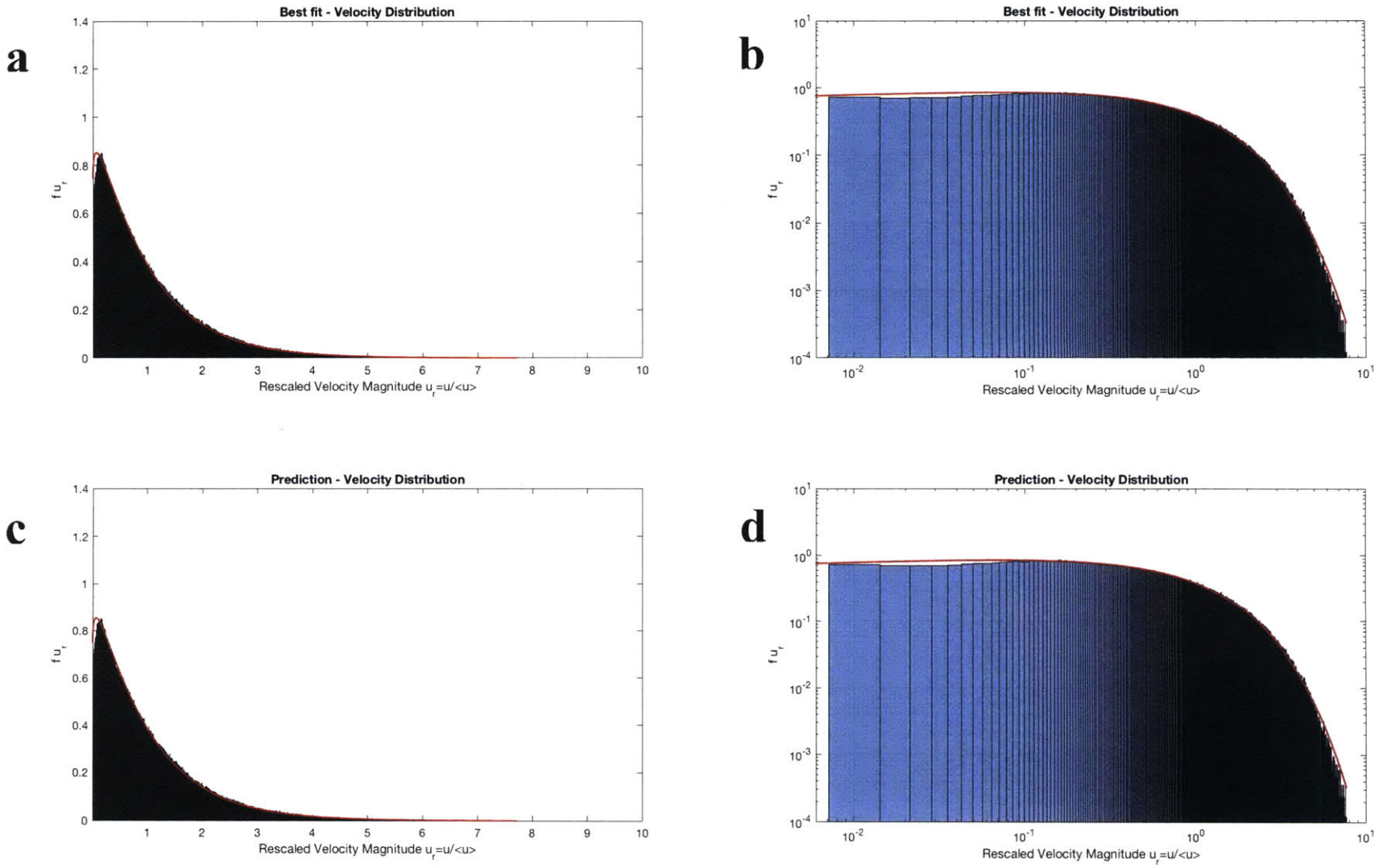

Figure A-12: For the 12th pack (a) Plot of the PDF of U_r (b) The same plot as (a) but in log-log scale. The red plot is the Gamma distribution with shape parameter that fit the PDF of U_r. In (c) and (d), the Gamma distribution with predicted value k has been used.

Bibliography

[1] Andrade, J. S., Jr., M. P. Almeida, J. M. Filho, S. Havlin, B. Suki, and H. E. Stanley (1997), Fluid flow through porous media: the role of stagnant zones, *Phys. Rev. Lett.*, 79, 3901-3904.

[2] Bear, J. (1972), *Dynamics of Fluids in Porous Media*, Elsevier, New York.

[3] Bijeljic, B., P. Mostaghimi, and M. J. Blunt (2011), Signature of non-Fickian solute transport in complex heterogeneous porous media, *Phys. Rev. Lett.*, 107, 204502.

[4] Blunt, M., and P. King (1990), Macroscopic parameters from simulations of pore scale flow, *Phys. Rev.* A, 42 (8), 4780-4787.

[5] Blunt, M. J. (2001), Flow in porous media - pore network models and multiphase flow, *Curr. Opin. Colloid Interface Sci.*, 6, 197-207.

[6] Blunt, M. J., et al. (2013), Pore-scale imaging and modelling, *Adv. Water Resour.*, 51, 97-216.

[7] Boisson, A., P. de Anna, O. Bour, T. Le Borgne, T. Labasque, and L. Aquilina (2013), Reaction chain modeling of denitrification reactions during a push-pull test, *J. Contaminant Hydrol.*, 148, 1-11.

[8] Bryant, S., P. R. King, and D.W. Mellor (1993), Network model evaluation of permeability and spatial correlation in a real random sphere packing, *Transp. Porous Media*, 11, 53-70.

[9] Cardenas, M. B. (2008), Three-dimensional vortices in single pores and their effects on transport, *Geophys. Res. Lett.*, *35*, L18402.

[10] Carman, P.C. (1937), Fluid flow through granular beds, *Trans. Inst. Chem. Eng., 15*, 150-166.

[11] Chen, C., A. I. Packman, and G. F. Gaillard (2008), Pore-scale analysis of permeability reduction resulting from colloid deposition, *Geophys. Res. Lett., 35* (7), L07404.

[12] Cueto-Felgueroso, L., and R. Juanes (2008), Nonlocal interface dynamics and pattern formation in gravity-driven unsaturated flow through porous media, *Phys. Rev. Lett.*, *101*, 244504.

[13] Dardis, O., and J. McCloskey (1998), Permeability porosity relationships from numerical simulations of fluid flow, *Geophys. Res. Lett., 25* (9), 1471-1474.

[14] Datta, S. S., H. Chiang, T. S. Ramakrishnan, and D. A. Weitz (2013), Spatial fluctuations of fluid velocities in flow through a three-dimensional porous medium, *Phys. Rev. Lett., 111*, 064501.

[15] de Anna, P., T. Le Borgne, M. Dentz, A. Tartakovsky, D. Bolster, and P. Davy (2013), Flow intermittency, dispersion and correlated continuous time random walks in porous media, *Phys. Rev. Lett.*, *101*, 184502.

[16] de Anna, P., M. Dentz, A. Tartakovsky, and T. Le Borgne (2014a), The filamentary structure of mixing fronts and its control on reaction kinetics in porous media flows, *Geophys. Res. Lett.*, *41* (13), 4586-4593.

[17] de Anna, P., B. Quaife, G. Biros and R. Juanes (2017), Porelets: Prediction of velocity distribution from pore structure in simple porous media, *Submitted for publication.*

[18] Dentz, M., A. Cortis, H. Scher, and B. Berkowitz (2004), Time behavior of solute transport in heterogeneous media: transition from anomalous to normal transport, *Adv. Water Resour.*, *27* (2), 155-173.

[19] Dentz, M., T. Le Borgne, A. Englert, and B. Bijeljic (2011), Mixing, spreading and reaction in heterogeneous media: a brief review, *J. Contaminant Hydrol.*, *120-121*, 1-17.

[20] Dullien, F. A. L. (1991), *Porous Media: Fluid Transport and Pore Structure*, second ed., Academic Press, San Diego, Calif.

[21] Durham, W., E. Climent, and R. Stocker (2011), Gyrotaxis in a steady vortical flow, *Phys. Rev. Lett.*, *106*, 238102.

[22] Fatt, I. (1956a), The network model of porous media I. Capillary pressure characteristics, *Petrol. Trans.* AIME, *207*, 144-159.

[23] Fatt, I. (1956b), The network model of porous media II. Dynamic properties of a single size tube network, *Petrol. Trans.* AIME, *207*, 160-163.

[24] Fatt, I. (1956c), The network model of porous media III. Dynamic properties of networks with tube radius distribution, *Petrol. Trans.* AIME, *207*, 164-181.

[25] Freeze, R. A., and J. A. Cherry (1979), *Groundwater*, Prentice Hall.

[26] Greengard, L., and V. Rokhlin (1987), A fast algorithm for particle simulations, *J. Comput. Phys.*, *73*, 325-348.

[27] Happel, J., and H. Brenner (1983), *Low Reynolds Number Hydrodynamics*, Martinus Nijhoff Publishers.

[28] Hofling, F., and T. Franosch (2013), Anomalous transport in the crowded world of biological cells, *Rep. Prog. Phys.*, *76* (4), 046602.

[29] Holzner, M., V. L. Morales, M. Willmann, and M. Dentz (2015), Intermittent Lagrangian velocities and accelerations in three-dimensional porous medium flow, *Phys. Rev. E, 92,* 013015.

[30] Icardi, M., G. Boccardo, D. L. Marchisio, T. Tosco, and R. Sethi (2014), Pore-scale simulation of fluid flow and solute dispersion in three-dimensional porous media, *Phys. Rev. E, 90*, 013032.

[31] Jha, B., L. Cueto-Felgueroso, and R. Juanes (2011), Fluid mixing from viscous fingering, *Phys. Rev. Lett., 106*, 194502.

[32] Kandhai, D., D. Hlushkou, A. G. Hoekstra, P. M. A. Sloot, H. V. As, and U. Tallarek (2002), Influence of stagnant zones on transient and asymptotic dispersion in macroscopically homogeneous porous media, *Phys. Rev. Lett., 88*, 234,501.

[33] Kang, P. K., P. de Anna, J. P. Nunes, B. Bijeljic, M. J. Blunt, and R. Juanes (2014), Pore-scale intermittent velocity structure underpinning anomalous transport through 3-D porous media, *Geophys. Res. Lett., 41* (17), 6184-6190.

[34] Kang, P. K., T. Le Borgne, M. Dentz, O. Bour, and R. Juanes (2015), Impact of velocity correlation and distribution on transport in fractured media: field evidence and theoretical model, *Water Resour. Res., 51* (2), 940-959.

[35] Kozeny, J. (1927), Uber kapillare leitung der wasser in boden, *Sitzungsber. Akad. Wiss. Wien, 136*, 271-306.

[36] Kutsovsky, Y. E., L. E. Scriven, H. T. Davis, and B. E. Hammer (1996), NMR imaging of velocity profiles and velocity distributions in bead packs, *Phys. Fluids, 8* (4), 863-871.

[37] Le Borgne, T., M. Dentz, and J. Carrera (2008), Lagrangian statistical model for transport in highly heterogeneous velocity fields, *Phys. Rev. Lett., 101*, 090601.

[38] Le Borgne, T., M. Dentz, P. Davy, D. Bolster, J. Carrera, J. R. de Dreuzy, and O. Bour (2011), Persistence of incomplete mixing: A key to anomalous transport, *Phys. Rev. E, 84*, 015301.

[39] Le Borgne, T., M. Dentz, and E. Villermaux (2013), Stretching, coalescence and mixing in porous media, *Phys. Rev. Lett., 110*, 204501.

[40] Le Borgne, T., M. Dentz, and E. Villermaux (2014), The lamellar description of mixing in porous media, *J. Fluid Mech., 770*, 458-498.

[41] Lebon, L., L. Oger, J. Leblond, J. P. Hulin, N. S. Martys, and L. M. Schwartz (1996), Pulsed gradient NMR measurements and numerical simulation of flow velocity distribution in sphere packings, *Phys. Fluids, 8* (2), 293-301.

[42] Levy, M., and B. Berkowitz (2003), Measurement and analysis of non-Fickian dispersion in heterogeneous porous media, *J. Contaminant Hydrol., 64*, 203–226.

[43] Manz, B., L. F. Gladden, and P. B. Warren (1999), Flow and dispersion in porous media: Lattice-Boltzmann and NMR studies, *AIChE Journal, 45* (9), 1845–1854.

[44] Matyka, M., J. Go lembiewski, and Z. Koza (2016), Power-exponential velocity distributions in disordered porous media, *Phys. Rev. E, 93*, 013110.

[45] Itasca Consulting Group Inc (2007), Particle Flow Code 3D, Version 4. 0, Itasca Consulting Group, Minneapolis, Minn, USA.

[46] W. M. Visscher and M. Bolsterli (1973), Random packing of equal and unequal spheres in two and three dimensions, *Nature*, *239*, 504–507.

[47] G. Mason and D. W. Mellor (1995), Simulation of drainage and imbibition in a random packing of equal spheres, *J. Colloid Interf. Sci., 176*(1), 214–225.

[48] E. M. Tory, N. A. Cochrane, and S. R. Waddell (1968), Anisotropy in simulated random packing of equal spheres, *Nature*, *220*, 1023–1024.

[49] L. Cui and C. O'Sullivan (2003), Analysis of a triangulation based approach for specimen generation for discrete element simulations, *Granular Matter*, *5*(3), 135–145.

[50] C. Geuzaine and J.-F. Remacle (2009). Gmsh: a three-dimensional finite element mesh generator with built-in pre- and post-processing facilities. *Int. J. Numer. Meth. Eng., 79*(11), 1309-1331.

[51] H. G. Weller, G. Tabor, H. Jasak, C. Fureby (1998), A tensorial approach to computational continuum mechanics using object-oriented techniques, *Comput. Phys. 12*(6), 620-631.

[52] S. Patankar (1980), *Numerical Heat Transfer and Fluid Flow*, CRC Press.

[53] S. V. Patankar and D. B. Spalding (1972), A calculation procedure for heat, mass and momentum transfer in three-dimensional parabolic flows, *Int. J. Heat Mass Transfer*, 15, 1787-1806.

[54] Ferziger, J.H., Peric, M. (2002), *Computational Methods for Fluid Dynamics*, 3rd ed., Springer, Berlin.

[55] Ayachit, U. (2015), *The ParaView Guide: A Parallel Visualization Application*, Kitware.

[56] J. H. van der Linden, G. A. Narsilio, A. Tordesilla (2016), Machine learning framework for analysis of transport through complex networks in porous, granular media: A focus on permeability, *Phys. Rev. E*, *94*(2), 022904.

[57] Le Borgne, T. Dentz, M., and Villermaux, E. (2015), The lamellar description of mixing in porous media. *J. Fluid Mech.*, *770*, 458–498.